NTNU
Norwegian University of
Science and Technology

Part A: Investigations of Sodium-Graphite Interaction

Part B: Structures and conformational Energies of 1,2- Dihaloethane and Silane Analogues

Part C: Development of Ab Initio computational Methods based on non-orthogonal Slater Determinants

Eirik Hjertenæs

Chemistry
Submission date: August 2011
Supervisor: Henrik Koch, IKJ

Norwegian University of Science and Technology
Department of Chemistry

Preface

This thesis has been submitted for the degree of Master of Science with specialization in Structural Chemistry, at the Norwegian University of Science and Technology, NTNU, Trondheim. The work has been carried out under the supervision of Henrik Koch and Reidar Stølevik between January 2010 and August 2011.

The thesis consists of three separate projects. This reports begins with an Introduction that presents the general quantum mechanical theory that is central to all three projects. Then each project is presented separately. Part A is called "Investigations of sodium-graphite interaction using quantum chemical methods". This work is a preliminary study for theoretical investigations that will be part of the DURAMAT-project (Durable Materials in Primary Aluminium Production).

Part B is an investigation of conformational energies and geometries of 1,2-dihaloethanes, halo(halomethyl)silanes and 1,2-dihalodisilanes.

Part C, Development of ab initio computational methods based on non-orthogonal Slater determinants, describes work done to implement and test a quantum chemical method developed by H. Koch and E. Dalgaard in 1993 in Dalton.

Abstracts

Part A

Cathode wear is the limiting factor in the lifetime of electrolytic cells in aluminium production. One important reason for wear in carbon cathode materials is the penetration and diffusion of sodium from the melt, through the cathode materials. A long-term goal is to use quantum chemistry methods to investigate this phenomenon on an atomic scale. In order to investigate large systems, density functional theory (DFT) must be applied. A small model system was considered, and calculations using various density functionals were compared to high level *ab initio* results. The comparison shows that TPSS is the best suited functional for sodium-graphite interactions. Using this functional, a larger system consisting of two coronene molecules and a sodium atom has been investigated and diffusion coefficients have been calculated based on harmonic transition state theory. Results show that calculated diffusion coefficients match experimental observations well, but also confirm that the model system considered is not large enough to describe bulk graphite.

Part B

Halogenated alkanes is a group of molecules that has received much attention, both in experiments and theoretical investigations. Here we focus on the 1,2-dihaloethanes. The restricted rotation around the C-C bond leads to a mixture of two rotamers, anti and gauche. Experiments and previous theoretical results show which conformer is lowest in energy depends on the substituted halogen, gauche is the preferred conformer for fluoro-substituted molecules, while anti is lowest in energy for the other halogens. This is attributed to steric repulsion. In order to further investigate this phenomenon, the geometries of 1,2-difluoroethane and 1,2-dichloroethane are optimized at the CCSD(T)/cc-pVDZ level. By replacing one or both of the carbon atoms by silicon, the corresponding halo(halomethyl)silane and 1,2-dihalodisilanes are formed. These molecules are also investigated using the same methods. Structural parameters and conformational energies are compared to experimental observations and theoretical results from literature. Results from calculations correspond well with experiments (for the molecules where experimental values are available) and with previous calculations (in the case of silane analogues). As predicted, the accuracy of the calculations increase when including electron correlation (MP2 and CCSD(T)) compared to the results from HF.

Part C

A computational method using wave functions constructed as a linear combination of *non-orthogonal* Slater determinants is proposed in an article by Koch and Dalgaard in 1993. Removing the requirement of orthogonality leads to a much more flexible wave function and more electron correlation can be recovered by using fewer determinants. The

method is implemented in Dalton. Test calculations for systems where FCI results are available shows the method has favourable performance compared to MP2 and CCSD(T).

Sammendrag

Del A

Slitasje i katodematerialer er den begrensende faktoren i levetiden til elektrolyseceller brukt i aluminiumsproduksjon. En årsak til slitasje er inntrengning og diffusjon av natrium i karbonmaterialer i katoden. Et langsiktig mål er å bruke kvantekjemiske metoder til å undersøke dette fenomenet på atom-nivå. For å gjennomføre beregninger på store system må man ta i bruk tetthetsfunksjonal-metoder, DFT. Et lite modellsystem er undersøkt med både DFT og nøyaktige *ab initio* metoder. En sammenligning mellom de ulike funksjonalene og CCSD(T) resultatene er gjort og basert på resultatene konkluderes det med at TPSS er det funksjonalet som best beskriver natrium-grafitt interaksjoner. Med dette funksjonalet er beregninger på et større modellsystem bestående av to coronen-molekyl og et natrium atom gjennomført. Fra potensialenergioverflate er diffusjonskonstanten bestemt ved hjelp av harmonisk overgangstilstand teori (HTST). Resultatene viser at estimerte diffusjonskonstanter stemmer godt overens med eksperimentelle observasjoner, men bekrefter også at et større system trengs for å beskrive diffusjon gjennom bulk grafitt.

Del B

Halogensubstituerte alkaner er en gruppe molekyl som har blitt grundig undersøkt gjennom eksperiment og teoretiske beregnigner. I denne studien fokuserer vi på 1,2-dihaloetan. Rotasjon rundt C-C bindingen fører til to isomerer, anti og gauche. Hvilken isomer som er lavest i energi har blitt undersøkt i både eksperiment og i teoretiske beregninger. Resultatene viser at den energimessig laveste isomeren avhenger av hvilket halogen som er subsitutert. I fluorsubsituterte molekyl er gauche den viktigste rotomeren, mens for de andre halogenene er anti den laveste i energi. Denne observasjonen forklares med sterisk frastøtning mellom subsitutentene. For å videre undersøke dette fenomenet er geometriene til 1,2-difluoroetan og 1,2-dikloroetan optimert med CCSD(T)/cc-pVDZ. I tillegg er silane-ekvivalentene (halo(halometyl)silan og 1,2-dihalodisilan) undersøkt for å avdekke mulige trender i konformasjonsenergier. Bindingslengder, vinkler og energiforskjeller mellom isomerene for hvert molekyl er beregnet og sammenlignet med eksperimentelle observasjoner (hvor tilgjengelig) og teoretiske beregninger i literaturen. Resultatene viser god oversetmmelse i begge tilfeller. Som forventer viser resultat fra CCSD(T) og MP2 høyere nøyaktighet enn HF-beregningene.

Del C

En beregningsmetode hvor bølgefunksjonen konstrueres som en lineær kombinasjon av *ikke-ortogonale* Slater determinanter (NOSD) er beskrevet av Koch og Dalgaard in en artikkel fra 1993. Ved å ikke kreve at determinantene må være ortogonale oppnås en mer fleksibel bølgefunksjon og elektronkorrelasjon kan beskrives ved bruk av færre determinanter enn i andre metoder. Metoden er implementert i Dalton og testet. Beregninger på system hvor FCI-resultat er tilgjengelig viser at meto-

den har fordeler sammenlignet med MP2 og CCSD(T).

Acknowledgments

I would like to thank my advisor, professor Henrik Koch, for his guidance and support during the work presented in this thesis. Working with the three projects described here, over the last two years, has been both interesting and challenging. I look forward to working with Dr. Koch the next four years as a PhD-candidate.
In Part A and B of this thesis, I have also worked with Stefan Andersson from SINTEF and Professor Reidar Stølevik. I would like to thank them both for the help they have given me.
I also want to express my gratitude towards the whole physical chemistry group at NTNU. The professors and PhD-candidates in the group all contribute to a great working environment, and are always willing to help when it is needed.
Last but not least, I want to thank my family and my girlfriend for all their support and encouragement.

Contents

List of Figures

List of Tables

List of Abbreviations

ADF Amsterdam Density Functional program

B3LYP Becke, 3-parameters, Lee-Yang-Parr. DFT-functional

BFGS Broyden-Fletcher-Goldfarb-Shanno. Optimization routine

BO Born-Oppenheimer

BSSE Basis Set Superposition Error

CBS Complete Basis set Limit

CC Coupled Cluster

CI Configuration Interaction

CP Counterpoise Correction

D3 Dispersion correction to DFT by Grimme et al.

DBE 1,2-dibromoethane

DCE 1,2-dichloroethane

DFE 1,2-difluoroethane

DFT Density Functional Theory

DIE 1,2-diiodoethane

FC Frozen Core

FCI Full Configuration Interaction

GGA Generalized Gradient Approximation

GTO Gaussian Type Orbitals

HF Hartree-Fock

HTST Harmonic transition state theory

KS Kohn-Sham

L-BFGS Limited memory BFGS

LDA Local Density Approximation

LSDA Local Spin-Density Approximation

MP2 Second order Møller-Plesset perturbation theory

NOSD Non-orthogonal Slater determinants

SE Schrödinger Equation

STO Slater Type Orbitals

SVD Singular value decomposition

TPSS Tao, Perdew, Staroverov and Scuseria. DFT functional

TST Transition state theory

Theoretical background

Chapter 1

Quantum mechanics of molecular systems

In this section I will give a brief introduction to the theoretical basis of this project. The nomenclature is adopted from *Modern Quantum Chemistry* by Szabo and Ostlund [1] and Helgaker et al. [2]. The majority of the theory is found in these two sources. Sections and equations found elsewhere are referenced explicitly. Throughout the thesis I will use atomic units to simplify the notation. A derivation of atomic units can be found in [3].

1.1 The Schrödinger equation

In quantum mechanics, the state of a system is represented by a wave function, denoted by Ψ. The evolution of the state with time follows the time dependent Schrödinger equation (SE) [1]:

$$i\frac{d\Psi(\mathbf{r},t)}{dt} = \hat{H}(\mathbf{r},t)\,|\Psi(\mathbf{r},t)\rangle \tag{1.1.1}$$

Here, $\hat{H}$ is the Hamiltonian operator corresponding to the total energy of the system, including any applied external fields. $|\Psi\rangle$ is the wave function, which according to the Copenhagen interpretation [4], contains all the information about a given state. In many cases, the Hamiltonian of a system is independent of time. One can then separate the time- and space-dependence of Equation (1.1.1) to yield the time independent Schrödinger equation:

$$\hat{H}\,|\Psi\rangle = E\,|\Psi\rangle \tag{1.1.2}$$

In Equation (1.1.2), E is the numerical value of the energy, given relative to the state where all electrons and nuclei are infinitely separated. The Hamiltonian operator of a molecular system has to include terms representing the kinetic energy of the electrons, T_e, the kinetic energy of the nuclei, T_n, potential energy from electron-electron repulsion, V_{ee}, nuclei-nuclei repulsion, V_{nn} and the electron-nuclei attraction, V_{ne}. A non-relativistic form of the Hamiltonian for a system with no external field is given by:

$$\hat{H} = -\frac{1}{2}\sum_{i=1}^{N_e}\hat{\nabla}_i^2 - \frac{1}{2}\sum_{I=1}^{N_n}\frac{\hat{\nabla}_I^2}{m_I} + \frac{1}{2}\sum_{i,j=1}^{N_e}\frac{1}{r_{ij}} + \frac{1}{2}\sum_{I,J=1}^{N_n}\frac{Z_I Z_J}{r_{IJ}} - \sum_{i=1}^{N_e}\sum_{J=1}^{N_n}\frac{Z_J}{R_{iJ}} \tag{1.1.3}$$

Here, lower case indices are used for electrons and upper case for nuclei. N_e is the total number of electrons and N_n is the number of nuclei. Z denote nucleic charges and m is the mass of a nucleus (relative to the mass of an electron).

For any system with more than two particles, Schrödingers equation with the Hamiltonian operator given by Equation (1.1.3) becomes intractable and almost impossible to solve analytically. The field of molecular quantum mechanics rely heavily on approximations in order to calculate the energy of even simple systems. Perhaps the most

indispensable approximation in quantum mechanics was proposed in 1927 by Born and Oppenheimer.

1.1.1 The Born-Oppenheimer approximation

The Born-Oppenheimer (BO) approximation is based on the observation that the mass of the nuclei is much greater than that of an electron (a proton is 1837 times heavier than an electron). It was therefore proposed that the electrons are able to respond instantaneously to movement of the nuclei, while the nuclei will respond very slowly to movement of the electrons. The wave function can then be written as

$$\Psi(r, R) = \phi_e(r; R)\Phi_N(R) \tag{1.1.4}$$

The notation $\phi_e(r; R)$ means that the electronic wave function depends on the nuclear position parametrically. The electronic Schrödinger equation becomes

$$T_e\phi_e + V\phi_e = E_e(R)\phi_e \tag{1.1.5}$$

Solving Equation (1.1.5) gives an electronic energy which depends on the position of the nuclei. This can then be used to calculate the total energy of the system

$$T_N\Phi + E_e\Phi = E\Phi \tag{1.1.6}$$

Using the procedure outlined here for many different conformations will give a potential energy surface for a polyatomic molecule. Equilibrium conformations and energies are found by locating the minima on this surface.

1.2 The electronic Schrödinger equation

Although the BO-approximation has simplified the problem of molecular calculations considerably, we are still left with the non-trivial task of solving the electronic Schrödinger equation. The approaches to solving the electronic Schrödinger equation are divided into two main branches, *ab initio* (or first principles) and semi-empirical methods. Semi-empirical methods use a simplified Hamiltonian and adjustable parameters obtained from experiments. In *ab initio* methods, a model wave function is chosen and the Schrödinger equation is solved using this wave function as the only input. The accuracy of the result depends on the quality of the chosen wave function. The computational cost is higher for *ab initio* methods, but their accuracy exceeds that of semi-empirical methods. In this project we use *ab initio* methods. A brief description of the methods we have used is given in section 1.5.

1.2.1 Molecular orbitals

Many of the most used methods in quantum chemistry are based on molecular orbital theory. Early discoveries in quantum mechanics gave good expressions for atomic orbitals for many-electronic atoms. Molecular orbital theory is based on using the atomic orbitals as starting points for molecular orbitals. An example is the construction of the molecular orbitals of H_2 from the 1s-atomic orbitals from hydrogen. The algebraic approach to solving the Schrödinger equation is based on building approximations to the wave function from such molecular orbitals.

Each electron in a molecule is assigned a one-electron function, called a spin orbital χ. Spin orbitals are products of the spatial one-electron functions and a spin-function, σ which is a function of one discrete variable, ω. The spin orbitals then depend on four variables, spatial coordinates and spin, which are usually gathered in the term $\mathbf{x}$.

$$\chi(\mathbf{x}) = \chi(x, y, z)\sigma(\omega) \tag{1.2.1}$$

A molecular orbital is then constructed as a linear combination of known one-electron functions

$$\phi_i = \sum_{\mu=1}^{N} c_{\mu i}\chi_\mu \tag{1.2.2}$$

1.2.2 The exact wave function

For any system larger than the hydrogen molecule ion, H_2^+, the form of the exact wave function is unknown. However, certain characteristics of the exact wave function is known. Any approximate wave function should share these characteristics.

Anti-symmetry

The experimental atomic spectrum of Helium shows only half of the states predicted by theory. The only states visible are those that are anti-symmetric with respect to interchange of any two electrons. This was recognized by Wolfgang Pauli, and is called Pauli's principle of anti-symmetry. From this, we know that the exact wave function must be anti-symmetric with respect to interchange of electrons. For a many-electron system, the simplest way of expressing a wave function which obeys this principle is in the form of a determinant, usually called a Slater determinant. A general form of such a determinant for a system with N electrons is given by:

$$\Psi(\mathbf{x_1}, \mathbf{x_2}, ..., \mathbf{x_N}) = \frac{1}{\sqrt{N!}} \begin{vmatrix} \phi_i(\mathbf{x_1}) & \phi_j(\mathbf{x_1}) & \cdots & \phi_k(\mathbf{x_1}) \\ \phi_i(\mathbf{x_2}) & \phi_j(\mathbf{x_2}) & \cdots & \phi_k(\mathbf{x_2}) \\ \vdots & \vdots & \ddots & \vdots \\ \phi_i(\mathbf{x_N}) & \phi_j(\mathbf{x_N}) & \cdots & \phi_k(\mathbf{x_N}) \end{vmatrix} \quad (1.2.3)$$

Interchanging two electrons in the wave function will be equivalent to switching two rows in the determinant, which results in a change of sign. Slater determinants are adopted in many applications of quantum mechanics for molecular systems today.

The variational principle

According to the variational principle, any normalized approximation to the wave function, that fulfills the boundary conditions of the system, will give an eigenvalue of the Hamiltonian that is an upper bound of the exact ground state energy. In other words, the energy calculated from an approximate wave function is always higher than the true energy. The variational method uses this principle, by employing a wave function that depends on parameters. By changing these parameters to minimize the energy, the best approximation to the wave function is found. For a generic trial function, ψ_{trial}, the Rayleigh ratio is defined as

$$\varepsilon = \frac{\int \psi^*_{trial} H \psi_{trial} d\tau}{\int \psi^*_{trial} \psi_{trial} d\tau} \quad (1.2.4)$$

The minimum value of the Rayleigh ratio will create and upper bound for the true ground state energy.

Size consistency

When describing a system built up of several non-interacting parts, it is clear that the total energy of the system should be equal to the sum of the individual particles. This has to hold because they are by definition non-interacting. An example could be a dimer, consisting of two monomers infinitely separated. Methods that obey this criterion are said to be size consistent. The exact wave function is obviously size consistent and therefore, any approximation should be as well. For many methods, this requirement is fulfilled, such as Hartree-Fock, but for others, it is not, such as truncated configuration interaction.

1.3 Second Quantization

In the original formulation of quantum mechanics, states are represented by functions, observables as operators and their numerical values as eigenvalues. An alternative formulation has been developed, where the wave functions are also represented by operators. The concept of a *vacuum state* is important. This is a state with no electrons. The wave function of any state is represented by a series of *creation* operators act on the vacuum state. A creation operator places an electron in a given orbital. The adjoint of a creation operator is an *annihilation* operator which removes an electron from the same orbital.

1.3.1 Second quantization states

A wave function in first quantization is typically represented by a Slater determinant, as in Equation (1.2.3). The equivalent expression in second quantization is considerably simplified. We introduce an abstract linear vector space, the *Fock space*, where a determinant is represented by a occupation number vector $|\mathbf{k}\rangle$

$$|\mathbf{k}\rangle = |k_1, k_2, \ldots, k_M\rangle \, , k_p = \begin{cases} 1 & \text{if} \quad \phi_p \quad \text{is occupied} \\ 0 & \text{if} \quad \phi_p \quad \text{is unoccupied} \end{cases} \tag{1.3.1}$$

Above, k_p is the occupation number of ϕ_p. It is 1 if ϕ_p is present in the determinant and 0 if not.

1.3.2 Creation- and annihilation-operators

Any state $|\mathbf{k}\rangle$ can be created by operating on the vacuum state with a series of creation operators according to

$$|\mathbf{k}\rangle = \prod_{p=1}^{M} \left(a_p^\dagger\right)^{k_p} |\text{vac}\rangle \tag{1.3.2}$$

Here, $|\text{vac}\rangle$ is $|0_1, 0_2, \ldots, 0_M\rangle$.

Acting on any vector $|\mathbf{k}\rangle$ with any creation operator yields:

$$a_p^\dagger \, |\mathbf{k}\rangle = \delta_{k_p 0} \Gamma_p^k \, |k_1, k_2, \ldots, 1_p, \ldots, k_M\rangle \tag{1.3.3}$$

In Equation (1.3.3), $\Gamma_p^k = \prod_{q=1}^{p-1} (-1)^{k_q}$, is a phase factor. It is apparent that operating with $a_p^\dagger$ on $|\mathbf{k}\rangle$ yields zero if the spin orbital ϕ_p is already occupied, since two electrons cannot occupy the same orbital. If the orbital was unoccupied, its occupation number changes from 0 to 1, in the occupation number vector. Acting on an occupation number vector with an annihilation operator is similarly defined

$$a_p \, |\mathbf{k}\rangle = \delta_{k_p 1} \Gamma_p^k \, |k_1, k_2, \ldots, 0_p, \ldots, k_M\rangle \tag{1.3.4}$$

Based on Equations (1.3.3)and (1.3.4), we can develop anti-commutator relations for the creation and annihilation operators. Knowing these

anti-commutators will greatly simplify many important equations encountered in molecular quantum mechanics.

$$a_p^\dagger a_q^\dagger + a_q^\dagger a_p^\dagger = \left[a_p^\dagger, a_q^\dagger\right]_+ = 0 \tag{1.3.5}$$

$$a_p a_q + a_q a_p = \left[a_p, a_q\right]_+ = 0 \tag{1.3.6}$$

$$a_p^\dagger a_q + a_q a_p^\dagger = \left[a_p^\dagger, a_q\right]_+ = \delta_{pq} \tag{1.3.7}$$

Some basic operators

All the important operators in quantum mechanics are derived from creation and annihilation operators. Three of the most basic are the occupation number operator, the particle number operator and the excitation operator.
The *occupation number operator* is defined as $\hat{N}_p = a_p^\dagger a_p$. When operating on a vector, it returns the number of electrons occupying spin orbital p, 0 or 1. The *particle number operator* is the sum of occupation number operators and returns the number of occupied spin orbitals in the determinant (or entries equal to 1 in the occupation number vector). The operator is given by:

$$\hat{N} = \sum_{p=1}^{M} a_p^\dagger a_p \tag{1.3.8}$$

The excitation operator excites an electron from spin orbital q to spin orbital p.

$$\hat{X}_q^p = a_p^\dagger a_q \tag{1.3.9}$$

When the excitation operator operates on a vector, the result is zero if the spin orbital q is unoccupied or if the spin orbital p is occupied.

1.3.3 The Hamiltonian operator

The coordinate representation of first quantization and the operator representation of second quantization leads to very different mathematical expressions. However, the expectation values corresponding to the same observable should be identical. In second quantization, the expectation value of an operator is written as a sum of matrix elements of operators. These values are required to be identical to their first quantization counterparts. A molecular electronic Hamiltonian operator in the Born-Oppenheimer approximation contains both one-electron and two-electron operator terms. The following section will outline how general one and two-electron operators are constructed.
In first quantization, a general one-electron operator for our system, can be written as a sum of operators as follows

$$f^c = \sum_{i=1}^{N} f^c(\mathbf{x}_i) \tag{1.3.10}$$

The superscript c indicates that we are working in the coordinate description of first quantization. The summation is over the N electrons in the system, adding one operator for each electron. All the operators in the sum depend only on their respective electron. Each term contains only reference to one electron and therefore any matrix elements between Slater determinants differing in more than one pair of spin orbitals will vanish. Thus the second quantization expression can be constructed as

$$\hat{f} = \sum_{pq} f_{pq} a_p^\dagger a_q \tag{1.3.11}$$

The two-electron equivalents are given as

$$g^c = \sum_{i \neq j}^{N} g^c(\mathbf{x}_i, \mathbf{x}_j) \tag{1.3.12}$$

in first quantization and as

$$\hat{g} = \frac{1}{2} \sum_{pqrs} g_{pqrs} a_p^\dagger a_r^\dagger a_s a_q \tag{1.3.13}$$

in second quantization. These are the pieces needed to construct the second quantization form of the molecular electronic Hamiltonian.

$$\hat{H} = \sum_{pq} h_{pq} a_p^\dagger a_q + \frac{1}{2} \sum_{pqrs} g_{pqrs} a_p^\dagger a_r^\dagger a_s a_q + h_{nuc} \tag{1.3.14}$$

The matrix elements h_{pq} and g_{pqrs} are found through the Slater-Condon rules for evaluating matrix elements in first quantization [5, 6]. They are given by

$$h_{pq} = \int \phi_p^*(\mathbf{x}) \left(-\frac{1}{2}\nabla^2 - \sum_I \frac{Z_I}{r_I} \right) \phi_q(\mathbf{x}) d\mathbf{x} \tag{1.3.15}$$

$$g_{pqrs} = \int \int \phi_p^*(\mathbf{x}_1) \phi_r^*(\mathbf{x}_2) \frac{1}{r_{12}} \phi_q(\mathbf{x}_1) \phi_s(\mathbf{x}_2) d\mathbf{x}_1 d\mathbf{x}_2 \equiv (pq|rs) \tag{1.3.16}$$

And the nuclear contribution is given by

$$h_{nuc} = \frac{1}{2} \sum_{I \neq J} \frac{Z_I Z_J}{R_{IJ}}$$

In the rest of this thesis, we will adopt the second quantization formulation and refer to states as occupation number vectors, or *kets*, $|\rangle$.

1.4 Orbital rotations

The choice of basis to express an occupation number vector is not unique. If we have one complete orthonormal basis $\{\phi_i\}$, it can be used to express any other state in another complete orthonormal basis $\{\varphi_j\}$. Since the basis $\{\phi_i\}$ is complete, we write a state in the basis $\{\varphi_j\}$ as follows

$$|\varphi_j\rangle = \sum_i |\phi_i\rangle \langle\phi_i|\varphi_j\rangle = \sum_i U_{ij} |\phi_i\rangle \tag{1.4.1}$$

$\mathbf{U}$ is then the matrix of the transformation. A reverse of the transformation above, would use the conjugate transpose of $\mathbf{U}$, $\mathbf{U}^\dagger$. Since the basis is orthonormal, the matrix $\mathbf{U}$ is unitary and we can write $\mathbf{U}\mathbf{U}^\dagger = 1$. Using this we know that we can always perform unitary transformations between different sets of spin orbitals, a feature that proves necessary in many applications such as electronic optimizations. In the following section we show that the matrix exponential of an anithermitian matrix yields unitary matrices. First, the matrix exponential is defined as

$$e^{\mathbf{A}} = \sum_{n=0}^{\infty} \frac{\mathbf{A}^n}{n!} = \mathbf{I} + \mathbf{A} + \frac{1}{2!}\mathbf{A}^2 + \dots \tag{1.4.2}$$

The matrix exponential is thus a matrix of the same dimensions as $\mathbf{A}$. Consider the antihermitian matrix $\imath\kappa$ and the relation from Equation (1.4.2)

$$e^{\imath\kappa} \left[e^{\imath\kappa}\right]^\dagger = e^{\imath\kappa} \left[e^{-\imath\kappa^\dagger}\right] = 1 \tag{1.4.3}$$

Thus $e^{\imath\kappa}$ is a unitary matrix, since $\kappa^\dagger = \kappa$. The unitary matrix of a transformation is equivalent to the operator $e^{\imath\hat{\kappa}}$. A unitary transformation of a reference state $|\Psi\rangle$, $e^{\imath\hat{\kappa}} |\Psi\rangle = |\tilde{\Psi}\rangle$, results in the following expression

$$e^{\imath\hat{\kappa}} |\Psi\rangle = e^{\imath\hat{\kappa}} a_1^\dagger a_2^\dagger \dots a_n^\dagger |\text{vac}\rangle \tag{1.4.4}$$

Since the exponential matrix is unitary, we can insert the product of the transformation matrix and its conjugate transpose between the creation operators

$$e^{\imath\hat{\kappa}} |\Psi\rangle = e^{\imath\hat{\kappa}} a_1^\dagger \left[e^{\imath\hat{\kappa}} e^{-\imath\hat{\kappa}}\right] a_2^\dagger \left[e^{\imath\hat{\kappa}} e^{-\imath\hat{\kappa}}\right] \dots \left[e^{\imath\hat{\kappa}} e^{-\imath\hat{\kappa}}\right] a_n^\dagger \left[e^{\imath\hat{\kappa}} e^{-\imath\hat{\kappa}}\right] |\text{vac}\rangle \tag{1.4.5}$$

We can now introduce the definition

$$\tilde{a}_r^\dagger = e^{\imath\hat{\kappa}} a_r^\dagger e^{-\imath\hat{\kappa}} \tag{1.4.6}$$

Thus we can write the transformed state in terms of a new set of transformed creation operators

$$e^{\imath\hat{\kappa}} |\Psi\rangle = \tilde{a}_1^\dagger \tilde{a}_2^\dagger \dots \tilde{a}_n^\dagger |\text{vac}\rangle \tag{1.4.7}$$

Equation (1.4.6) can be expressed in terms of commutators, using the Baker-Campbell-Hausdorff expansion [7–10],

$$\begin{aligned} e^{\mathbf{A}} \mathbf{B} e^{-\mathbf{A}} = \mathbf{B} + [\mathbf{A}, \mathbf{B}] + \frac{1}{2!} [\mathbf{A}, [\mathbf{A}, \mathbf{B}]] \\ + \frac{1}{3!} [\mathbf{A}, [\mathbf{A}, [\mathbf{A}, \mathbf{B}]]] + \dots \end{aligned} \tag{1.4.8}$$

With the equations in this section, we are able to evaluate the transformed state $|\tilde{\Psi}\rangle$ in terms of the untransformed creation operators.

1.5 Computational methods

1.5.1 The Hartree-Fock self-consistent field method

In Section 1.2.2 we introduced the concept of variationality and the Rayleigh ratio (Equation (1.2.4)). Imagine a reference state $|\text{ref}\rangle$, which is a single Slater determinant. If an orbital rotation $e^{\imath\kappa}$ is applied as described in Section 1.4, we obtain a wave function $|\kappa\rangle$. The variational parameters in this state is the choice of spin orbitals, thus we vary the matrix κ and minimize the energy

$$E = \min_{\kappa} \langle\kappa|\hat{H}|\kappa\rangle \tag{1.5.1}$$

Within the Born-Oppenheimer approximation, the complicating factor in computational chemistry is the electron correlation. In the Hartree-Fock (HF) method, each electron is considered to be moving in an average potential field created by the nuclei and the $n-1$ other electrons. Thus, each spin orbital is assumed to be an eigenfunction of the one-particle operator $\hat{f}$, the Fock operator.

$$\hat{f} = \hat{h} + \hat{V}_{HF} \tag{1.5.2}$$

where $\hat{h}$ is the one electron term of the Hamiltonian from Equation (1.3.14) and $\hat{V}_{HF}$ is the HF mean field potential given by

$$\hat{V}_{HF} = \sum_{pq}^{all} \sum_{i}^{occupied} (g_{pqii} - g_{piiq}) a_p^\dagger a_q \tag{1.5.3}$$

For a system of n electrons we thus have a system of n equations, that depend on each other. Because of this dependence, the problem has to be solved iteratively, i.e. in a self-consistent field (HF-SCF).

The HF method is adopted as the basis of many more advanced computational methods and it is therefore used to define the term *electron correlation energy*. The electron correlation energy is defined as the difference between the exact non-relativistic energy and the HF energy of the system

$$E_{corr} = E_{exact} - E_{HF} \tag{1.5.4}$$

Within the BO approximation, the only error in the HF-energy is the electron correlation energy, and the goal of most post-HF methods is to recover as much of the electron correlation as possible.

1.5.2 Møller-Plesset perturbation theory

Møller-Plesset perturbation theory is a variation of Rayleigh-Schrödinger perturbation theory. The zero-order Hamiltonian is taken as the Fock operator, $\hat{H}^0 = \hat{f}$. The first order perturbation of the Hamiltonian is given by

$$\hat{H}^1 = \hat{H} - \hat{f} - \hat{h}_{\text{nuc}} \tag{1.5.5}$$

where H is the electronic Hamiltonian. If we use the groun dstate HF wave function, Φ_0 and standard perturbation theory we arrive at

$$E_0^{(0)} = \langle \Phi_0 | \hat{f} | \Phi_0 \rangle = \sum_i \varepsilon_i \tag{1.5.6}$$

$$E_0^{(1)} = \langle \Phi_0 | \hat{H}^1 | \Phi_0 \rangle \tag{1.5.7}$$

$$E_0^{(2)} = -\frac{1}{4} \sum_{ijab} \frac{|g_{aibj} - g_{ajbi}|^2}{\varepsilon_a + \varepsilon_b - \varepsilon_i + \varepsilon_j} \tag{1.5.8}$$

Second order Møller-Plesset perturbation theory (MP2) is one of the simplest methods which includes electron correlation. Because of its

simplicity, it is a popular method for large systems. The MP2 energy is given by

$$E_{MP2} = E_{HF} - \frac{1}{4}\sum_{ijab}\frac{|g_{aibj} - g_{ajbi}|^2}{\varepsilon_a + \varepsilon_b - \varepsilon_i + \varepsilon_j} \tag{1.5.9}$$

1.5.3 Configuration interaction

The method of configuration interaction, CI, is conceptually very simple. It is based on the fact that the exact ground state wave function can be expressed as a linear combination of all the possible n-electron Slater determinants, using a complete set of spin orbitals [11].

$$|CI\rangle = \sum_i C_i |i\rangle \tag{1.5.10}$$

Although the idea is quite simple, the method is not feasible in practice, since it involves a sum over *all* possible n-electron Slater determinants and a complete infinite basis set. The number of determinants needed for a system of n electrons using a basis set of M functions, $2M$ spin orbitals is given by $\begin{pmatrix} 2M \\ n \end{pmatrix}$. For a system with 10 electrons and 20 basis set functions, which by today's standards is considered a small system, the number of determinants then reaches a total of

$$\begin{pmatrix} 2M \\ n \end{pmatrix} = \begin{pmatrix} 40 \\ 10 \end{pmatrix} = 8.477 \times 10^8$$

Thus the number of states included in the sum in Equation (1.5.10) is always truncated. Despite this truncation and the following deviation from the exact wave function CI is a commonly used method. Its biggest advantage is its description of bond breaking. However, because of the truncation, the method is not size consistent and is therefore not suitable for polymolecular systems, such as dimers.

1.5.4 Coupled Cluster theory

The treatment of electrons without electron correlation is referred to as the independent particle model. The description of a molecular system consists of a wave function (a product of creation operators acting on a vacuum state), represented by a set of occupied spin orbitals. Coupled cluster (CC) theory attempts to improve this description by expressing the interaction of electrons as excitations from occupied to virtual orbitals. Each excitation has its amplitude, or the probability of such an excitation resulting from electron interactions. In the simplest sense, we consider two electrons in a molecular system interacting, and the interaction leading to an excitation of both to different spin orbitals

$$a_i^\dagger a_j^\dagger \rightarrow a_i^\dagger a_j^\dagger + \sum_{a>b} t_{ij}^{ab} a_a^\dagger a_b^\dagger \tag{1.5.11}$$

For occupied orbitals, summation indexes I,J,K,... are usually used, while A,B,C,... represent virtual orbitals. The quantity t_{ij}^{ab} is the amplitude associated with the pair excitation. We define the operator

$$\hat{\tau}_{ij}^{ab} = a_a^\dagger a_i a_b^\dagger a_j \tag{1.5.12}$$

Coupled cluster uses the Hartree-Fock wave function as a reference state, and we can thus write the coupled cluster wave function with double excitations, CCD, as

$$|CCD\rangle = \left[\prod_{\substack{a>b \\ i>j}} \left(1 + t_{ij}^{ab}\hat{\tau}_{ij}^{ab}\right)\right] |HF\rangle \tag{1.5.13}$$

A more general form of the coupled cluster wave function with all levels of excitation allowed (single, double, triple, etc) can be written in terms of the previously defined excitation operator

$$|CC\rangle = \left[\prod_{a,i}\left(1+\hat{X}_i^a\right)\right]\left[\prod_{\substack{a>b\\ i>j}}\left(1+\hat{X}_{ij}^{ab}\right)\right]\ldots|HF\rangle \tag{1.5.14}$$

Since $\hat{X}_i^a\hat{X}_i^a = 0$ and $\left[\hat{X}_i^a, \hat{X}_j^b\right] = 0$, the expression above can be rewritten as

$$|CC\rangle = exp\left(\sum_{a,i} t_i^a \hat{X}_i^a + \sum_{\substack{a>b\\ i>j}} t_{ij}^{ab}\hat{X}_{ij}^{ab} + \ldots\right)|HF\rangle = e^{\hat{T}}\,|HF\rangle \tag{1.5.15}$$

The coupled cluster operator $\hat{T}$ is a non Hermitian operator, consisting of a sum of terms each corresponding to excitations (single, double, triple, ect)

$$\hat{T} = \hat{T}_1 + \hat{T}_2 + \hat{T}_3 + \ldots \tag{1.5.16}$$

The sum in $\hat{T}$ can be truncated at any point and this has given rise to a series of methods with increasing accuracy as the number of terms included increase (coupled cluster singles (CCS), coupled cluster singles and doubles (CCSD), etc). CCSDT is a highly accurate method, but the cost of including all the triple excitations is very high. In order to capture some of electron correlation without the cost of including all triple excitations, a hybrid method called CCSD(T) has been developed. Here, the single and double excitations are included in the full extent, while the triple excitations are calculated using perturbation theory. Because of this methods compromise between accuracy and computational costs, it is considered the *gold standard* of computational chemistry. For a more thorough discussion of the method, see [12].

1.6 Basis sets

In Section 1.2.1, we referred to known one-electron functions (Equation (1.2.2)). These known functions are collected in sets of functions called basis sets, which contain atom-specific one-electron functions. Basis sets are typically discussed in terms of their size, meaning the number of functions used to describe each orbital. By using a large basis set one can obtain increased accuracy, but the computational cost will be increased. Basis sets are designed for specific applications and many different types have been developed.
The first basis functions that were used, were Slater-type orbitals (STOs). These were the first choice because of their excellent fit with true atomic orbitals. However, STOs are computationally demanding and today, the majority of the common basis sets use Gaussian type orbitals (GTOs), where a number of Gaussian functions are fitted to a Slater-type orbital. The smallest basis sets are referred to as minimal basis sets. One common type of minimal basis set are the STO-nG sets. Here, n Gaussian functions are fitted to a single STO. The small basis sets are normally only used for very large systems, where computational restrictions demand it, or for preliminary calculations. They are rarely good enough to obtain chemical accuracy, 1 kcal/mol.

1.6.1 Split valence basis sets

To increase the accuracy of a basis set, additional functions are included in the description of each orbital. Adding functions makes the wave function fit better with the true orbitals. Every function added increases the computational cost. The improvement of the accuracy relative to computational cost has been shown to be best when adding functions to the valence orbitals. The effect of increasing the description of core orbitals leads to less gain in accuracy. Basis sets with added functions for the valence orbitals are called split-valence ba-

sis sets and these are most commonly used to day. In Part A of this thesis we have used Dunning's correlation-consistent-polarized valence basis sets [13] with diffuse functions added. These sets are called *aug-cc-pVnZ*. *aug* is short for augmented and implies the use of diffuse functions. n is the cardinal number which denotes how many functions are used for valence orbitals. Commonly used values of n is $2-6$. For $n = 2$, the basis set is denoted *double zeta* etc. In Part B, basis sets of the type cc-pVnZ are used. These are the same as in Part A, but without the diffuse functions.

1.6.2 Basis set extrapolation

In order to obtain an exact description of true spin orbitals, a complete infinite basis set has to be used. This is called the *basis set limit*. It is of course not feasible to use an infinite basis in an actual calculation, and we always have to accept a certain *basis-set truncation error*. Increasing the basis sets leads to an improvement of the calculated energy and in the limit of an infinite basis set we approach the basis set limit energy. If a series of calculations are performed with increasing basis set size, it has been shown that the calculated energies converge towards the basis set limit [14]. This has given rise to formulas for basis set extrapolation. If the same calculation is carried out using a double- and triple-zeta basis set, these energies can be used to predict the quadruple-zeta energies [15]. In this project an extrapolation scheme which extrapolates the electron correlation energy has been used:

$$
\begin{aligned}
x &= D = 2 \\
y &= T = 3 \\
xy &= Q = 4 \\
E_x &= E_x^{HF} + E_x^{corr} \\
E_y &= E_y^{HF} + E_y^{corr} \\
E_{xy}^{corr} &= \frac{E_x^{corr} \times x^3 - E_y^{corr} \times y^3}{x^3 - y^3} \\
E_{xy}^{HF} &\approx E_y^{HF} \\
E_{xy} &= E_y^{HF} + \frac{E_x^{corr} \times x^3 - E_y^{corr} \times y^3}{x^3 - y^3}
\end{aligned}
$$

Above, D and T denote the number of valence functions in the two basis sets (double and triple zeta).

1.6.3 Basis set superposition error

Basis set superposition error (BSSE) is a common source of errors when doing calculations on systems with multiple molecules. For such systems, the property of interest is often the binding energy, or the relative energy of the system with atoms at a given separation, compared to the sum of the atomic energies, infitely separated. As atoms on different molecules approach each other, their basis functions overlap and are mixed. This mixing leads to an increased size of the effective basis set for the monomers. This in itself is not an error, but it leads to an inconsistency in the relative energy of the complex.
One common method for reducing the BSSE is counterpoise correction (CP) [16]. The interaction energy of a dimer AB with monomers A and B is typically calculated as

$$\Delta E_{int}(AB) = E_{AB}^{AB}(AB) - E_{A}^{A}(A) - E_{B}^{B}(B) \tag{1.6.1}$$

Where the superscripts denotes which basis set is used, subscripts denote the geometry considered, and the symbols in the parenthesis is the chemical system considered. In other words, one does three calculations, one of the dimer and one of each monomer by itself. For each monomer the goal is to correct for the artificial stabilization from the basis functions on the other monomer. This can be calculated as

$$E_{BSSE}(A) = E_{A}^{AB}(A) - E_{A}^{A}(A) \tag{1.6.2}$$

and similarly for B. Subtracting this correction from the uncorrected interaction energy gives

$$\Delta E_{int}^{CP}(AB) = E_{AB}^{AB}(AB) - E_{A}^{AB}(A) - E_{B}^{AB}(B) \tag{1.6.3}$$

In practice, the calculation of the dimer is done exactly as before, but in the calculations of the respective monomers, the basis functions of the other dimer is included as *ghost functions*. The nuclear charge and the electrons of the *ghost atoms* are ignored.

1.7 Midbond functions

In *ab initio* calculations, there is always an error in the electron correlation due to the limited basis set size. This is also true for investigations of multiple systems. When investigating systems of several molecules, there is also intermolecular correlation to consider. A method to solve this problem is the use of *midbond* functions. It has been shown that placing a set of Gaussian functions at the centre of a van der Waals bond, helps recover important electron correlation at a low computational cost [17]. In cases of symmetric interactions, the logical placement of the bond functions are at the centre of the bond.

For asymmetric interactions, one has to decide where to place the functions. Fortunately, investigations have shown that the movement of displacement of the midbond functions within reasonable limits has only a negligible effect on the interaction energy [17].

Chapter 2

Density functional theory

The high computational cost of the *ab initio* methods described in 1, has motivated the search for alternative methods. One branch is density functional theory (DFT). Instead of focusing on state functions, DFT focuses on the electron probability density, ρ. The Hohenberg-Kohn theorem presents the formal proof that the ground state energy and other ground state properties can be uniquely described by the electron density [18]. DFT is also based on the Born-Oppenheimer approximation. The electronic energy is said to be a functional of the electron density, $E[\rho(\mathbf{r})]$. However, the theorem only states that such a functional exists, its form is unknown. From the postulates of quantum mechanics, we know that the electron probability density is given by the square of the wave function. In DFT, electronic density is expressed as a linear combination of the squares of Kohn-Sham (KS) orbitals

$$\rho(\mathbf{r}) = \sum_{i=1}^{n} |\psi_i(\mathbf{r})|^2 \tag{2.0.1}$$

Using KS orbitals, the exact ground state energy can be expressed as

$$
\begin{aligned}
E[\rho] &= \sum_{i=1}^{n} \int \psi_1^*(\mathbf{r}_1) \nabla_1^2 \psi_1(\mathbf{r}_1) d\mathbf{r}_1 - j_0 \sum_{I=1}^{N} \frac{Z_I}{r_{I1}} \rho(\mathbf{r}_1) d\mathbf{r}_1 \\
&+ \frac{1}{2} j_0 \int \frac{\rho(\mathbf{r}_1)\rho(\mathbf{r}_2)}{r_{12}} d\mathbf{r}_1 d\mathbf{r}_2 + E_{XC}[\rho] \qquad (2.0.2)
\end{aligned}
$$

The term E_{XC} is the exchange-correlation potential. The exact form of this function is unknown. There are various types of DFT that use different approximations to this potential.

Applying the variational principle to the equations above, gives the Kohn-Sham equations, which yields the Kohn-Sham orbitals when solved iteratively. The KS orbitals are usually expressed in terms of a linear combination of known basis functions, similarly to HF. In fact, the same type of basis sets can be used in DFT as in *ab initio* methods.

The computational cost of DFT is much lower than that of post-HF methods. Using DFT allows the investigation of systems much larger than would have been possible with MP2 or CC, and it still accounts for some electron correlation. However, the density functionals used contain empirical elements in E_{XC}. In HF or post-HF methods, we know there is a hierarchy of methods with increasing accuracy. Consider for example CC; the CC-operator contains an infinite sum of excitations. The accuracy of the energy can systematically be improved by including more terms in the series. In DFT there is no such order because of the approximations in the exchange-correlation potential. As a result of this, functionals have to be calibrated against experimental results or first principles calculations. Calibration has to be done for specific types of systems, so that a functional is known to give good results for the system in question.

2.1 Functionals

As mentioned above, the greatest challenge with DFT is finding a suitable density functional. Since the method was proposed in 1964 [18], the development of density functionals has received much attention. There are several different types of density functionals available for DFT calculations today. The four most common types are

- Local density approximation - LDA
- Generalized gradient approximations - GGA
- meta-GGA
- Hybrid functionals

2.1.1 Local density approximation

The first functional to be suggested was the local density approximation, LDA. A functional of this type was proposed in one of the first DFT-articles in 1965 [19]. The exchange-correlation potential is expressed as

$$E_{XC}^{LDA}[n] = \int n(r)\varepsilon_{XC}\left(n(r)\right) d\mathbf{r} \tag{2.1.1}$$

Within the approximation that the electron density is slowly varying, the function $\varepsilon_{XC}\left(n(r)\right)$ can be estimated as the exchange and correlation energy per electron of a uniform electron gas. Methods based on this approach are classified as LDA-functionals. Newer methods that also depend on spin are called local spin-density approximations (LSDA).

$$E_{XC}^{LSDA}[n_\uparrow, n_\downarrow] = \int n(r)\varepsilon_{XC}\left(n_\uparrow(r), n_\downarrow(r)\right) d\mathbf{r} \tag{2.1.2}$$

These two types of functionals were the first to be developed and are the most primitive. We will not be using any of these types in this project.

2.1.2 Generalized gradient approximation

An improvement to the LDA approach is generalized gradient approximation functionals, GGA [20,21]. Like LDA, these functionals consider only the density at one point, but also depend on the gradient at this location. These functionals are also spin-dependent. The exchange-correlation potentials are of the form

$$E_{XC}^{GGA}[n_\uparrow, n_\downarrow] = \int n(r)\varepsilon_{XC}\left(n_\uparrow(r), n_\downarrow(r), \vec{\nabla}n_\uparrow(r), \vec{\nabla}n_\downarrow(r)\right) d\mathbf{r} \quad (2.1.3)$$

2.1.3 Meta-GGA

Functionals of the type Meta-GGA depend on the same factors as the GGA-functionals, but also include the second derivative of the density. A common example of this type of functional is developed by Tao, Perdew, Staroverov and Scuseria (TPSS) [22] in 2003. The general expression of the exchange-correlation functional is

$$E_{XC}^{meta-GGA}[n_\uparrow, n_\downarrow] = \int n(r)\varepsilon_{XC}\left(n_\uparrow(r), n_\downarrow(r), \vec{\nabla}n_\uparrow(r), \vec{\nabla}n_\downarrow(r), \tau_\uparrow, \tau_\downarrow\right) d\mathbf{r} \quad (2.1.4)$$

2.1.4 Hybrid potentials

Hybrid potentials are potentials that incorporate exchange and correlation energies from other methods, such as Hartree-Fock. The most

common hybrid potential is B3LYP (Becke, 3-parameter, Lee-Yang-Parr) [23]. This method uses the LDA exchange correlation potential and adds corrections as a linear combination with terms from GGA, LDA and HF

$$E_{XC}^{B3LYP} = E_{XC}^{LDA} + a_0 \left(E_X^{HF} - E_X^{LDA}\right) + a_x \left(E_X^{GGA} - E_X^{LDA}\right) + a_C \left(E_C^{GGA} - E_C^{LDA}\right) \quad (2.1.5)$$

The coefficients $\{a_n\}$ are empirical parameters fitted to experimental results.

2.2 Dispersion corrections

In the description of multi-molecular systems, dispersion forces play an important role. Unfortunately, van der Waals forces are one of the weaknesses of DFT. A number of corrections to this problem are suggested and one of the most promising are DFT-D corrections by Grimme et al. [24]. The newest generations are called DFT-D3 and these are used in our DFT calculations. This type of correction has been tested for many systems, including graphene sheets [24], which is particularly interesting for our calculations in Part A. The dispersion potential is calculated adding pair wise contributions to the dispersion forces. The dispersion coefficients are calculated from first principles and are not semi-empirical, thus they do not have to be parametrized. The total DFT energy including the dispersion correction can be written as

$$E_{DFT-D3} = E_{KS-DFT} - E_{disp} \quad (2.2.1)$$

where E_{KS-DFT} is usual DFT KS energy and E_{disp} is the dispersion correction. The dispersion correction consists of two terms, the two- and three-body contributions

$$E_{disp} = E^{(2)} + E^{(3)} \tag{2.2.2}$$

Of these two, the two-body term has the largest contribution. It is given by

$$E^{(2)} = \sum_{AB} \sum_{n=6,8,10,\ldots} s_n \frac{C_n^{AB}}{r_{AB}^n} f_{d,n}(r_{AB}) \tag{2.2.3}$$

The first summation runs over all the atom pairs in the molecule, while the second sums the nth order dispersion coefficients C_n^{AB} (only $n = 6, 8, 10, \ldots$) for pair AB. s_n are scaling factors for $n > 6$ that are used to ensure asymptotic exactness. $f_{d,n}$ are damping functions that define the range of each dispersion correction. They are given by

$$f_{d,n}(r_{AB}) = \frac{1}{1 + 6(\frac{r_{AB}}{(s_{r,n} R_0^{AB})})^{-\alpha_n}} \tag{2.2.4}$$

In Equation (2.2.4), $s_{r,n}$ are order-dependent scaling factors that adjust the cutoff radii, R_0^{AB}. α_n are "steepness" parameters, which are set manually. Typically, $\alpha_6 = 14$ and the other are given by $\alpha_{n+2} = \alpha_n + 2$.

Part A

Investigations of sodium-graphite interaction using quantum chemical methods

Chapter 3

Background and theory

3.1 Background for this project

The problems of cathode wear in aluminium production is the motivation behind a research project titled DuraMat - Durable materials in primary aluminium production. The project is a co-operation between Hydro, Sintef - Materials and Chemistry, and NTNU, with support from the Norwegian Research Council. Part of the project will revolve around sodium penetration and diffusion in the cathode materials, and will involve micro scale simulations. Part A of this thesis is a preliminary study for the DuraMat project.

3.2 Aluminium production

The dominating method for producing aluminium today, is the Hall-Héroult process [25]. Aluminum is electrolyzed from a molten aluminium flouride (Na_3AlF_6) electrolyte, with dissolved AlF_3 and Al_2O_3. The overall cell reaction is given by

$$2Al_2O_3 + 3C(s) \rightarrow 4Al(l) + 3CO_2(g) \tag{3.2.1}$$

The operating temperature of the cell is approximately 900-1000^{o}C. A hanging block of carbon is the anode of the cell. Strictly speaking, the molten metal pad is the cathode. However, throughout literature, the container of the aluminium and the electrolyte is called the cathode. This container is lined with prebaked carbon pieces, sealed with a paste. The carbon blocks are usually made of graphitic or graphitized carbon. The lifetime of a Hall-Héroult cell is limited by the lifetime of these carbon blocks. The repair and replacement of degraded carbon blocks represents a major cost in aluminium production both due to material costs and downtime. If the degradation and wear of the carbon cathode materials could be prevented, the aluminum industry could make considerable savings. Many measures have been investigated, but none have been completely effective [26]. There are several causes of the wear of the cathodes, one of them is the penetration and diffusion of sodium atoms from the electrolyte into the carbon material The mobility of sodium in carbon materials has been investigated both experimentally [27, 28] and simulated using mathematical models [29] but the underlying mechanisms are still unknown. In order to achieve a better understanding of the principles behind sodium diffusion in graphite, atomistic modeling is needed.

The problem of sodium degradation of carbon materials, can be divided into two parts: First, sodium adsorbed and penetrates into the carbon material. Secondly, the atoms diffuse in through the bulk material. Both aspects are of interest for the prevention of degradation of cathodes, and it is very likely that the mechanisms are coupled, i.e. once sodium has entered the graphite material, this lowers the energy barrier for further penetration. The former problem is quite complicated, involving an investigation of the interactions between sodium atoms and the boundary of a graphite-like material. This requires a

large model system and will be not be the focus in this project. In this work, we focus on the diffusion of sodium through the cathode, once it has entered.

3.3 DFT calibration

Using CC and MP2 theory as described in sections 1.5.4 and 1.5.2, the size of the feasible model system is very restricted. To investigate systems that are large enough to capture the nature of bulk graphite, DFT (Section 2) must be used. In order for the results from DFT calculations to be reliable, they must be calibrated. This will be the first part of this project. With the smallest realistic model system, we will calculate potential energy curves using high accuracy post-HF methods. The same calculations will be carried out using different types of DFT-functionals. The functional giving the best fit with the *ab initio* results will be used for the larger model systems.

3.4 Sodium diffusion

The movement of a sodium atom in a graphite lattice, is restricted to two dimensions, because sodium atoms are too large to penetrate the graphite sheets. In addition, for preliminary purposes, it is sufficient to assume that a sodium atom only interacts with the two closest carbon sheets. Based on this, the problem can be investigated using a simple model system, consisting of two graphite sheets and a few sodium atoms. The first simulations will use only one sodium atom. The model system will be expanded to include more sodium atoms at a later stage.
In a graphite lattice, the sodium atoms are stabilized when they are located in the sites formed by the six-membered carbon rings. The

movement from one site to a neighbouring one can be described by transition state theory (TST) [30]. Although TST is an approximation, it has shown to describe solid diffusion very well [31]. The principal idea behind TST is to locate a dividing surface, separating two minima (reactants and products) and estimating the flux through this surface. In a thermal ensemble, the TST rate constant, k^{TST}, is proportional to the probability of being at the dividing surface relative to the probability of being everywhere else. This eliminates the need to consider specific trajectories. A further approximation to TST is harmonic transition state theory (HTST) or Vineyard theory. HTST requires a defined saddle point along the reaction coordinate. The dividing surface is then a hyperplane perpendicular to the reaction coordinate at the saddle point. Further, one assumes that the vibrations around the energy minima are approximately harmonic. This must also hold for all the vibrational modes at the saddle point, except the mode that lies parallel to the reaction coordinate. A jump between sites requires an activation energy and the jump rate typically follows an Arrhenius law [32]

$$k^{HTST} = \nu^0 exp\left(-\frac{\Delta E_{barrier}}{k_B T}\right) \tag{3.4.1}$$

where, $\Delta E_{barrier}$ is the barrier height associated with a jump, k_B the Boltzmann constant, T the absolute temperature and the prefactor ν^0 is the attempt frequency. This frequency is of the order of the Debye frequency of the system and can be approximated as

$$\nu^0 = \frac{\prod_i^{3N} \nu_i^{min}}{\prod_j^{3N-1} \nu_j^{TS}} \tag{3.4.2}$$

Here, ν^{min} and ν^{TS} are the vibrational frequencies at the minimum and the transition state, respectively. The prefactor can be calculated from simulations or approximated. Throughout literature, the prefactor is

usually estimated to be of the order of $10^{12}-10^{13}$ [33,34]. The diffusion constant is then be given by

$$D = \frac{k^{HTST} d^2}{6} \tag{3.4.3}$$

Here, the factor $\frac{1}{6}$ enters from the hexagonal symmetry of the graphite lattice and d is the distance between two sites, known to be 1.4 Å. If the prefactor is approximated based on the type of lattice, the only value needed from simulations is the energy barrier. When the barrier is known, the diffusion coefficient can be calculated.

3.4.1 Experimental diffusion coefficients

The field of sodium diffusion in carbon materials has received much attention. There are many experimental studies that have measured the diffusion constant of sodium through graphite. The model systems considered in this study will be relatively small, and we do not expect the results to be accurate enough to compare against experimental results. However, we list some of the reported experimental values here.

Table 3.1: Experimentally determined diffusion coefficients of sodium in graphite and other carbon materials from literature

Reference	Temperature (K)	Material	Diffusion coefficient
Kozlov et al. [27]	773	Graphite	$2.6 - 5.0 \times 10^{-12}$
T. Naas [35]	1193	Semigraphite	$0.4 - 0.8 \times 10^{-9}$
T. Naas [35]	1243	Semigraphite	$0.5 - 1.2 \times 10^{-9}$
Houston et al. [36]	1003	Graphite	0.9×10^{-9}

3.5 Goals and hypothesis

An atomistic modeling of the penetration and diffusion of sodium through graphite materials requires a large model system. For this type of system, MP2 or CC calculations require too much computer resources. To investigate large systems, one must use DFT. The first goal of this part of the thesis is to conduct a calibration study. A system consisting of a sodium dimer and a benzene ring will be used for the calibration. This system is small enough to allow calculations at the CCSD(T)/aug-cc-pVTZ level(Sections 1.5. The same calculations will be conducted using various DFT-functionals. These will be evaluated against the CCSD(T)-results.

Once a suitable functional has been found, the second goal is to begin simulations with larger model systems. Using graphite-like molecules, we hope to find a good approximation of the energy barrier height of lattice jumps for sodium in graphite (Equation (3.4.1)). The focus will initially be on describing the movement of sodium through bulk graphite. The first model system will be two rigid coronene molecules with a sodium atom placed between them. The potential energy surface will be calculated by moving the sodium atom in two dimensions, while the coronene molecules are kept rigid at a fixed distance. This distance is set to the equilibrium distance. Using HTST we will calculate diffusion coefficients from the energy barriers.

Chapter 4

Computational methods

4.1 Calibration studies

4.1.1 Ab initio methods

The smallest system possible that would represent the graphite-sodium interactions in a good way was chosen to be a benzene ring and a sodium dimer. Although sodium is present in the electrolyte as both single atoms and dimers, Na_2 was used in the simulations. Calculations are carried out using MP2, CCSD and CCSD(T) methods. Coupled cluster methods are best suited for closed shell systems, while a benzene ring and a sodium atom would be a doublet state. The CCSD(T) calculation of such as system would result in a *spin contamination* which we would have to correct for. Because of this we decided to use the sodium dimer and thus eliminate spin contamination completely. Three different geometries were used (Figure 4.1); the two molecules in a parallel orientation with the center of the sodium-sodium bond aligned with the center of the benzene ring (Figure 4.1(a)), perpendicular orientation with the sodium-sodium bond pointing towards the center of the benzene ring (Figure 4.1(b)), and a parallel offset geom-

etry where the sodium-sodium bond parallel to the benzene ring, with one sodium atom located directly above the center of the benzene ring (Figure 4.1(c)).

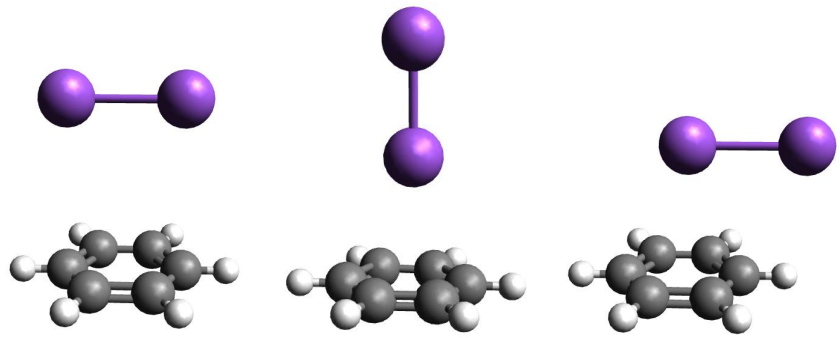

(a) Parallel geometry (b) Perpendicular geometry (c) Parallel offset geometry

Figure 4.1: (a), (b) and (c) show the three orientations of benzene and a sodium dimer that were investigated.

For all three geometries, the distance between the two molecules was varied, while the bonds were kept fixed, and a potential energy curve was plotted. Curves were plotted using MP2, CCSD and CCSD(T) methods and aug-cc-pVDZ and aug-cc-pVTZ. For the parallel orientation MP2/aug-cc-pVQZ energies were also calculated. For the other methods, the quadruple zeta basis set energies were obtained by extrapolations according to Equation (1.6.1). All result were counterpoise corrected and midbond functions were placed midway between the two molecules. All calculations were carried out using CFOUR [37].

4.1.2 DFT calculations

The same potential energy curves that were described in Section 4.1.1 were calculated using DFT. Ten different functionals were investigated, 8 of them with D3-corrections (Section 2.2). The functionals used are listed in Table 4.1. DFT calculations were carried out using the Amsterdam density functional program (ADF) [38]. Calculations with DFT on benzene and a sodium dimer in the parallel geometry were carried out by Stefan Andersson, SINTEF [39].

Table 4.1: List of the functionals used in the DFT-calibration

Type	Functional	with D3
GGA	BLYP	Yes
GGA	BP86	Yes
GGA	PBE	Yes
GGA	PBEsol	Yes
GGA	revPBE	Yes
GGA	RPBE	Yes
meta-GGA	TPSS	Yes
hybrid	B3LYP	Yes
meta-hybrid	M06	No
meta-hybrid	M06-2X	No

4.2 Double coronene potential surface

The smallest model system showing sufficient resemblance to a graphite lattice with intercalated sodium is a pair of coronene molecules with one sodium atom placed in between (Figure 4.2). The two coronene molecules were kept rigid at their equilibrium geometry during the simulations. The distance between the two molecules was optimized,

with a sodium atom placed right between the two centers of the middle benzene rings, and kept constant. The z-coordinate of the sodium atom was also kept fixed, in the middle of the two coronene molecules, while the position in the centre plane was varied. These calculations were done with ADF using a TZ2P basis set and the TPSS functional with D3 corrections (See Section 5.1 for a description of the performance of the functionals and the selection of the best one).

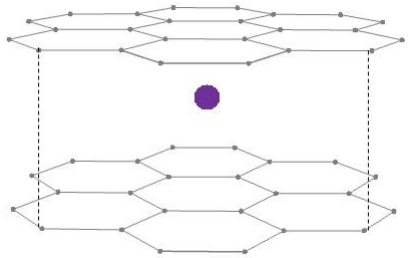

Figure 4.2: The model system used to generate a potential energy surface

Chapter 5

Results and discussion

5.1 DFT calibration

For each of the three geometries shown in Figure 4.1, potential energy curves were calculated using MP2, CCSD and CCSD(T) with aug-cc-pVXZ (X = D, T and Q) basis sets. The energy curves are shown in Figures 5.1- 5.3. In all the calculations, the sodium dimer and the benzene ring were kept rigid in their equilibrium geometry while their separation was varied. In these graphs we see that the energies calculated with MP2, CCSD and CCSD(T) follow the same trends for all three geometries. The binding energy calculated with MP2 is overestimated and the minimum distance is too short. The binding energy from CCSD is underestimated and the minimum distance is too long. The results from the CCSD(T) calculations lie between the two former methods in both binding energy and minimum distance. Within each method, increasing the size of the basis set leads to a lowering in energy. When comparing the potential energy curves for the tree geometries, the largest binding energy and the shortest minimum distance occurs for the perpendicular orientation. In this geometry, one

of the sodium atoms is placed directly over the ”hole” in the benzene ring. It is therefore equidistant from all six carbons. The other sodium atom is further away from the benzene ring. In this orientation, the molecules fit very well geometrically and this explains the increased binding energy compared to the other geometries.

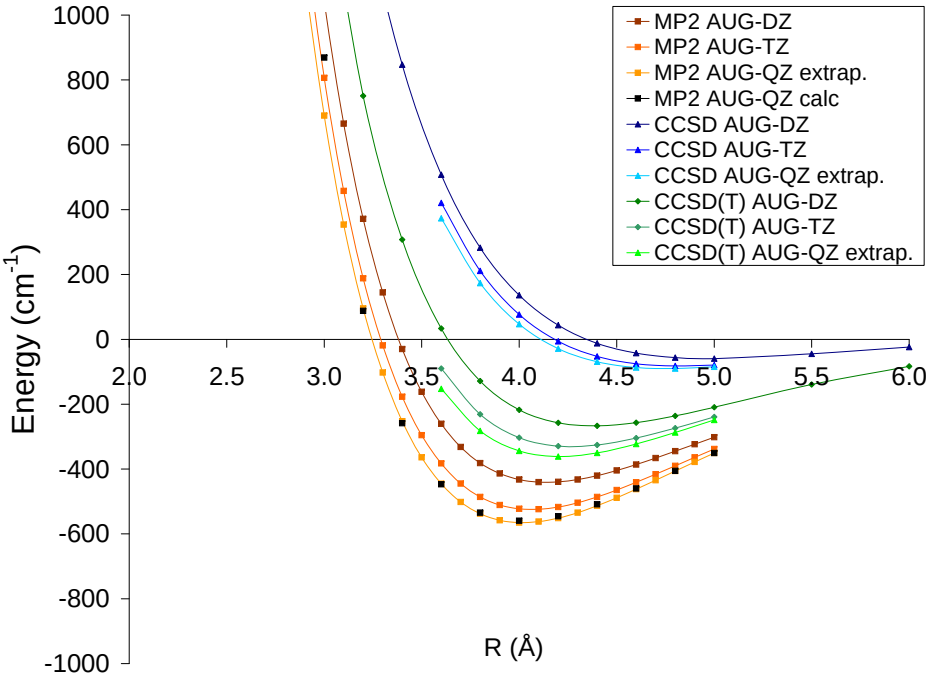

Figure 5.1: Potential energy curves for benzene and a sodium dimer in parallel geometry. The QZ energy is calculated only for MP2, and extrapolations from DZ and TZ energies for CCSD and CCSD(T).

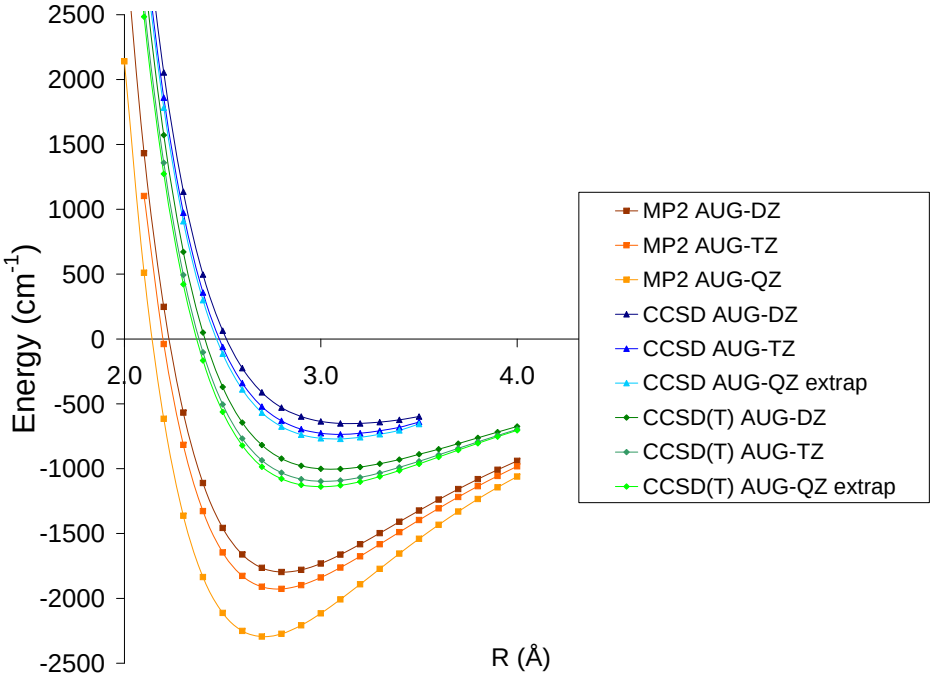

Figure 5.2: Potential energy curves for benzene and a sodium dimer in perpendicular geometry. The QZ energies are extrapolations from DZ and TZ-energies.

The same potential energy curves as in the previous section are calculated with DFT using all the functionals from Table 4.1. When comparing the DFT interaction energies to the CCSD(T), we assume that all three geometrical orientations are equally important. For each geometry, the standard deviation of the DFT energy of each functional in each point, with respect to the CCSD(T)/aug-cc-pVDZ energy is calculated according to Equation (5.1.1).

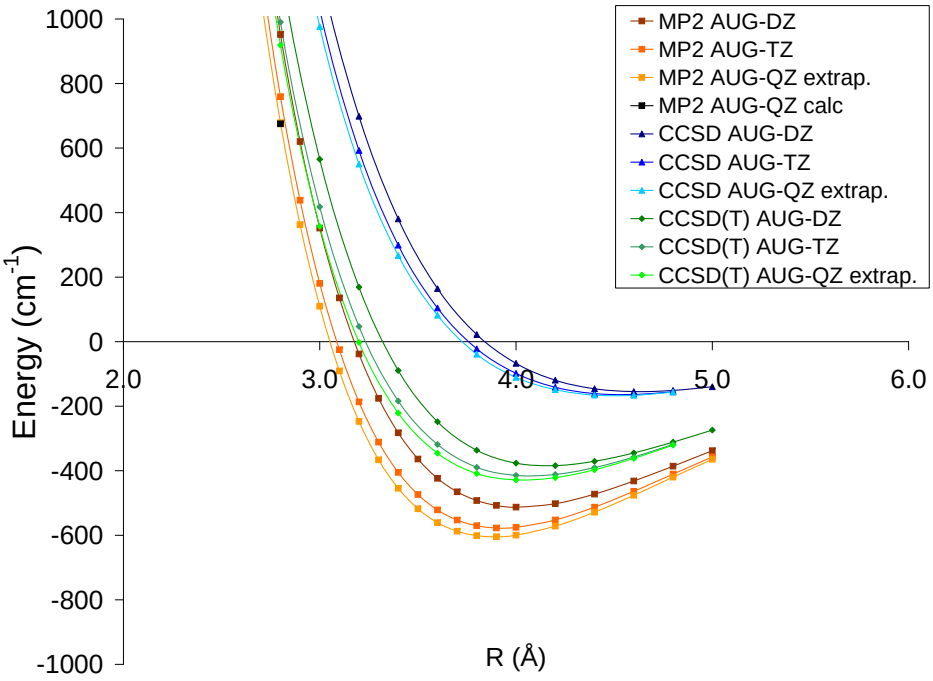

Figure 5.3: Potential energy curves for benzene and a sodium dimer in a parallel offset orientation. The QZ energies are extrapolations from DZ and TZ-energies.

$$\sigma = \frac{1}{n} \sum_{Geometries} \sum_{R} \sqrt{\left(E_{DFT}(R) - E_{CCSD(T)}(R)\right)^2} \tag{5.1.1}$$

Here, n is the number of observations. We consider five points in the region of the minima in binding energy in each geometry. This was used as a criteria for the evaluation of the DFT-functionals. In addition, we found the highest deviation from CCSD(T), in any geometry,

at any distance separation for each of the functionals. These results are summarized in Figure 5.4.

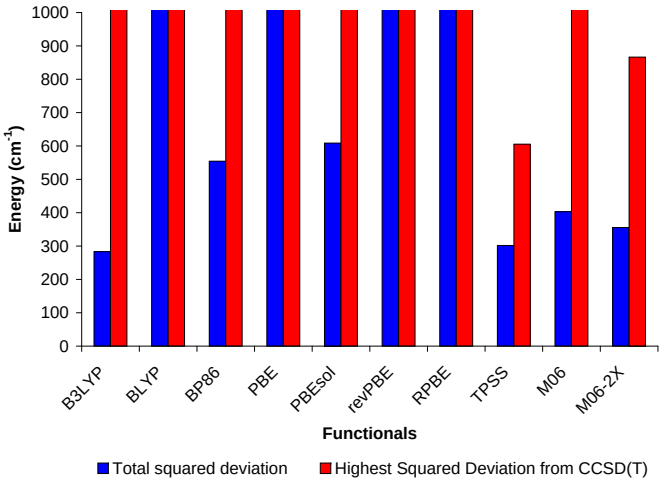

Figure 5.4: The standard deviation from CCSD(T)/aug-cc-pVTZ energy and the highest deviation in any point for each of the functionals in Table 4.1

We clearly see that there are large variations in the deviations from the CCSD(T)/aug-cc-pVTZ energies between the functionals. The best three functionals appear to be B3LYP-D3, M06-2X and TPSS-D3. The lowest maximum deviation from the CCSD(T)-curve in any point is found with the TPSS-functional, with an maximum error of approximately 600 cm^{-1}. This error is 55% of the total binding energy from CCSD(T)/aug-cc-pVTZ calculation. The lowest average deviation is found in B3LYP and TPSS, which both have errors of approximately 300 cm^{-1}, or 27% of the binding energy. The other functionals perform even worse in comparison and we do not show their potential

energy curves here (see Appendix A). In Figures 5.5- 5.7 the potential energy curves of the best three functionals are shown, along with the CCSD(T)/aug-cc-pVTZ energy, for each of the three geometries. All DFT calculations are carried out with the TZ2P basis set and B3LYP and TPSS are corrected with D3.

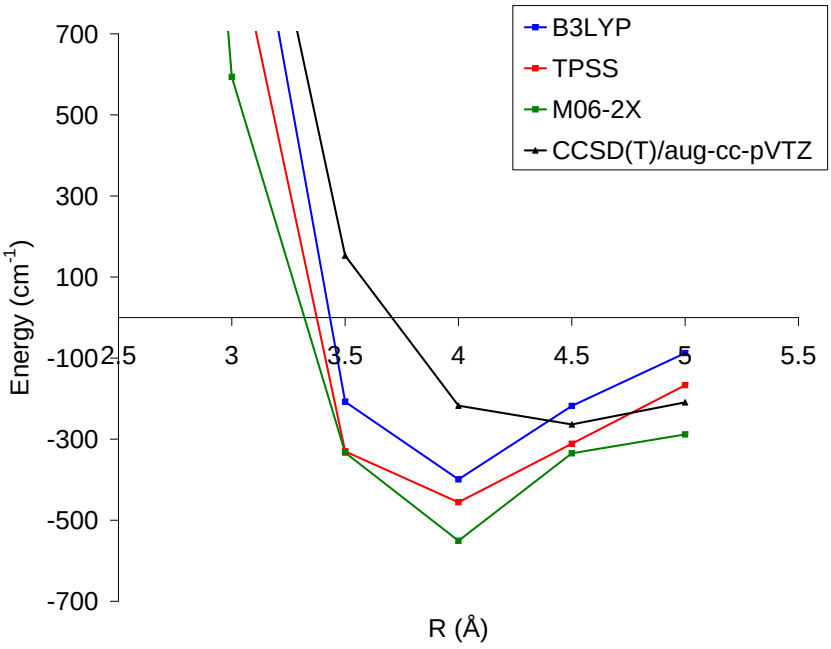

Figure 5.5: The DFT potential energy curves of benzene and a sodium dimer in the parallel geometry (Figure 4.1). B3LYP and TPSS calculations shown here were carried out by Stefan Andersson, SINTEF.

The standard deviation of M06-2X with respect to CCSD(T)/aug-cc-pVDZ energy curve is relatively low, however, the M06-2X curve displays a distinct bump around the minima for all three geometries. This hump is clearly un-physical and based on this, we chose to not

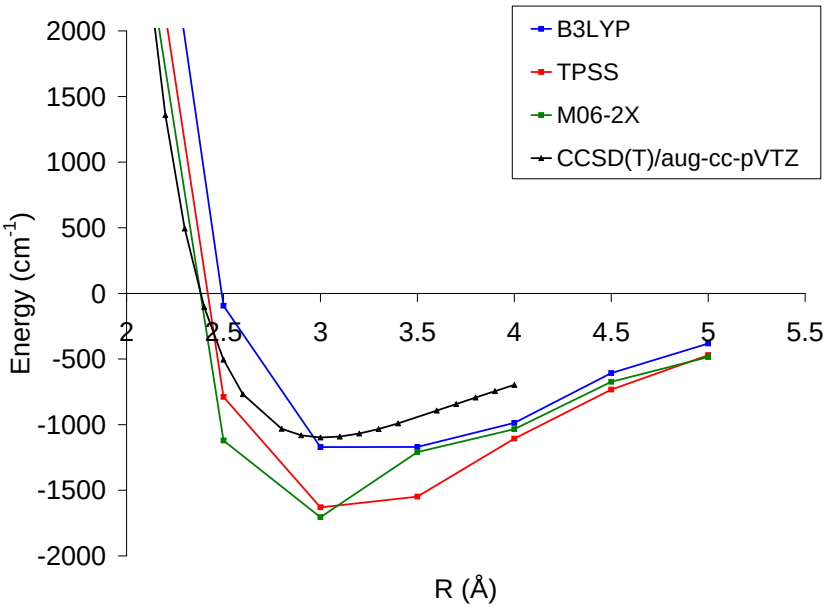

Figure 5.6: The DFT potential energy curves of benzene and a sodium dimer in the perpendicular geometry.

use this functional in our further investigations. When comparing the other two functionals to the CC result, there are several factors to consider. One is the numerical accuracy. According to Figure 5.4 the TPSS functional provides the best results in this respect. Another important factor is the congruency of the entire potential energy curve compared to that of CCSD(T). As mentioned in Section 3.4, the energy barrier of site-jumps is important for the calculation of the diffusion coefficients based on HTST. It will therefore be important to use a functional that describes the relative well-depth as accurately as possible. From the DFT potential energy curves it looks like B3LYP dis-

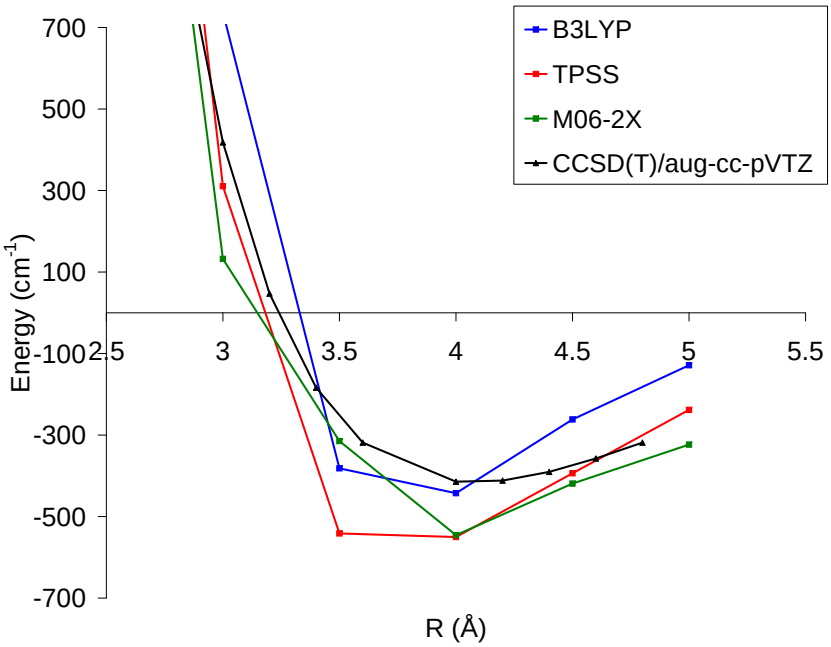

Figure 5.7: The DFT potential energy curves of benzene and a sodium dimer in the parallel offset geometry.

plays a better fit than TPSS, despite the observations from Figure 5.4.

Up to this point we have only discussed the relative performance of the DFT-functionals compared to each other. Our results show that B3LYP and TPSS perform considerably better than the others we have tested. It is also relevant to comment on the performance of these functionals in absolute terms. Let us consider the potential energy curves of the perpendicular orientation (Figure 5.6). The binding energy calculated from CCSD(T)/aug-cc-pVTZ is -1098 cm^{-1} and the equilibrium distance is 3 Å. TPSS predicts similar minimum distance

but overestimates the binding energy by almost 50%. The binding energy from B3LYP is considerably better, but it is still about 10% too low. The bonding distance predicted by B3LYP is also approximately 0.25 Å too long, an error of 8%. Both these functionals produce considerable errors both in binding distance and energy. Keeping in mind that the perpendicular orientation appears to be the one where DFT fits the best with the *ab initio* results, the overall performance is less than impressive.

5.2 Potential surface and energy barriers

Based on the results from the calibration study, we chose to begin calculations on the coronene-Na-coronene system with both B3LYP and TPSS. The first task was to determine the equilibrium distance between the coronene molecules to be used in the potential surface calculations. When varying the distance between the coronene molecules using B3LYP, the calculated potential energy curve displayed an unphysical bump or discontinuity. The same was seen in the preliminary calculations of the potential energy surface of the coronene-sodium-coronene system. The same calculations with TPSS gave smooth and continuous curves, we therefore decided to abandon B3LYP in our further investigations and rely only on TPSS. The equilibrium distance between the two coronene molecules, when a sodium is placed between them was determined to be 4.6 Å, 1.25 Å larger than the normal spacing of graphite sheets of 3.35 Å.

In Figure 5.8 the potential energy of a sodium atom moving between two rigid coronene molecules kept at a fixed separation of 4.6 Å is shown. The energy (cm^{-1}) is calculated with TPSS-D3/TZ2P. The

coronene molecules are oriented parallel to each other and such that the position of all the atoms are eclipsed. It is important to point out that the edge of the double coronene molecule is not intended to represent the surface of a graphite lattice. The part of the potential energy surface corresponding to the area outside the carbon framework of the system, will not be discussed here. As expected, our calculations show seven minima in the potential energy, each corresponding to a position in the middle of each of the six-membered carbon rings in the coronene molecules. In these locations, the sodium atom is separated by equal distances from all its 12 most neighbouring carbon atoms and the nuclear repulsion is minimized. Moving the sodium atoms between these minima brings it very close to the carbon atoms and leads to increased potential energy. This is equivalent to an energy barrier that has to be overcome. A perhaps unexpected observation, is that the energy of the minima in the central carbon ring is higher than those in the outer rings. It is difficult to explain exactly why this occurs. However, the difference between the outer and inner sites indicate that edge effects stabilize the former. This observation suggests that the test system is not big enough to describe bulk graphite material. In bulk graphite, we would expect all the sites to be of the same potential energy.
Another factor to consider, is that our test system contains only one sodium atom. The mechanisms behind sodium diffusion are not completely understood, however, it is highly likely that the sodium atoms interact with each other, while intercalated in the graphite lattice. Any such effects will not be described by our model. In Section 5.1 we discuss the inaccuracy of DFT-TPSS and we see a 50% error in the binding energy compared to CCSD(T)/aug-cc-pVDZ. This error is quite substantial and we must expect this to affect the energy barriers.
The observations described above, clearly illustrate the limitations of our small model system. To summarize, the system is too small to represent bulk graphite, it does not consider sodium-sodium interactions

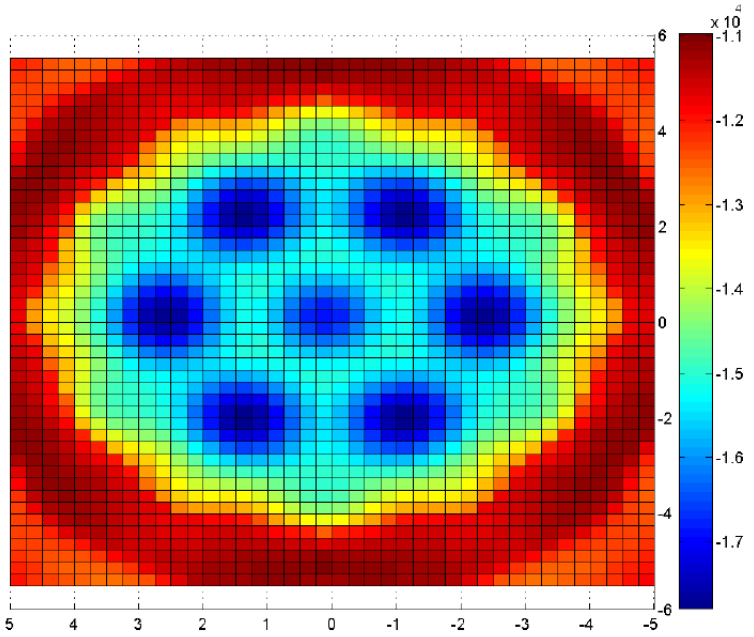

Figure 5.8: Potential energy surface of a sodium atom moving between two coronene molecules. Energies are in cm^{-1}. The surface is drawn in a cartesian coordinate system in units of Å, where the centre of the coronene molecules are placed at the origin.

and the penetration of sodium into the graphite material is not considered. Based on this, it may be optimistic to comparing the calculated diffusion coefficients to those reported from experiment in literature. Nevertheless, Figure 5.10 shows the diffusion coefficients from our calculations along with the values reported by [27,35,36]. Diffusion coefficients are calculated according to Equations (3.4.3) and (3.4.1). The energy barrier is found in the potential energy surface of a sodium atom moving between two coronene molecules (Figure 5.8) and a pref-

actor of $10^{12}s^{-1}$ is used. The experimental results are presented with their respective error bars. Because of the difference in the energy of the central site and the six outer, and the symmetry of the system, there are three unique barrier heights to consider (Figure 5.9).

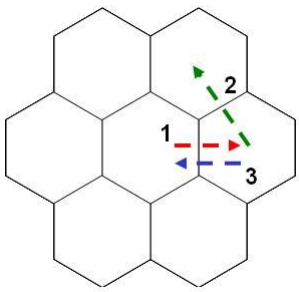

Figure 5.9: The three unique energy barriers in a coronene-sodium-coronene system

The energy barrier from each of the three jumps illustrated in Figure 5.9 are listed in Table 5.2. At this point we do not know which of the energy barriers are closest to that of real graphite, therefore diffusion coefficients are calculated for all three. The energy barriers will also be affected by the error in binding energy from the DFT-calculations, which could be as high as 50%.

Table 5.1: Barrier heights and diffusion coefficients

Barrier	Barrier height TPSS (eV)
1	0.208
2	0.287
3	0.321

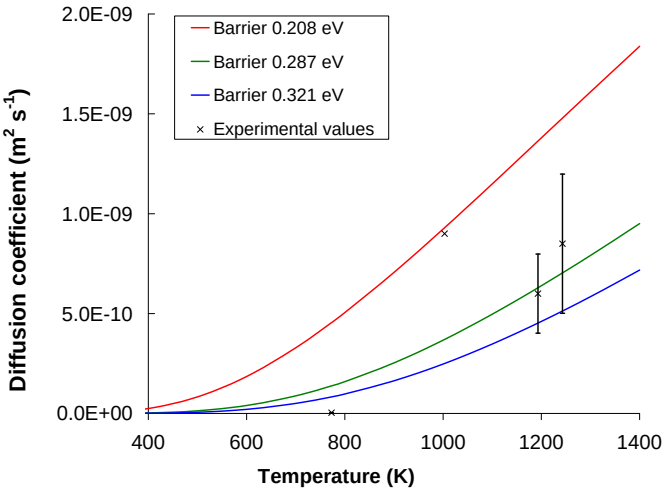

Figure 5.10: The variations in the diffusion coefficients with temperature. The three lines represent diffusion coefficients calculated from the three barrier heights from the DFT-D3/TPSS calculations. Experimental values from [27], [36] and [35] are included.

It appears that the results from our calculations correspond well with the experimental results, within our choice of exponential pre-factor. In particular the diffusion coefficients calculated from the two lowest energy barriers match the experimental values reported by Naas [35] very well. Considering all the limitations to our system, it is unlikely that this observation means that our calculations are very accurate. The logical explanation is rather that the limitations to our model system mentioned above, work in opposite directions, leaving the calculated diffusion coefficient on the same order of magnitude as the experimental results. For example, the initial penetration of sodium into the graphite lattice, leads to expansion and an increase in the

inter-layer separation [40]. This therefore represents an energy barrier decreasing the effective diffusion coefficient. At the same time, it is argued that the sodium-sodium interactions are cooperative [41], which would increase rate of diffusion through the lattice. Since our model disregards both these effects, we have calculated a diffusion coefficient that matches experiments well, by accident.

Chapter 6

Conclusions

In Chapter 5 the limitations and short-comings of our model system is discussed. At this point the calculated diffusion coefficients are unreliable, yet we have obtained results worth summarizing. We have successfully tested many of the state-of-the art density functionals for the interactions between sodium and aromatic organic compounds. The conclusion from this calibration study is that the TPSS functional with the DFT-D3 dispersion corrections is the most suitable functional. Although this functional performs better than the others that were tested, it matches CCSD(T)/aug-cc-pVTZ calculations quite poorly. A 50% divergence in the binding energy is considerable. This motivates us to continue to look for other functionals. If other functionals are found, they can easily tested against the *ab initio* results we have reported. Using the TPSS functional we have investigated an initial model system consisting of 48 carbon atoms and 1 sodium atom. Observations indicate that this system is too small to accurately describe sodium diffusion through graphite. However, the methodology applied in this project can and will be applied to larger model systems. We expect that by increasing the size of the model system, an accurate diffusion coefficient for the movement of sodium

through bulk graphite can be calculated. Altogether, the work presented here provides a good foundation for the further investigations of sodium-graphite interactions using quantum chemical methods in the DuraMat project.

Chapter 7

Future work

The work done in Part A of this thesis presents many directions for further work. The first and most obvious task is to expand the graphite-like model and calculate a new potential energy surface. An improvement would be to use ovalene (Figure 7.1) instead of coronene. The most important difference between ovalene and coronene is that ovalene has two equivalent central sites. The energy barrier between these, and how it compares with those from the coronene-Na-sodium experiments, will indicate whether a ovalene-Na-ovalene system is representative of bulk graphite.

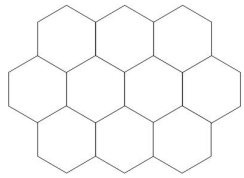

Figure 7.1: Ovalene

The DFT-calculations we have performed are relatively fast which means that we can also begin to look at even larger model molecules

than ovalene. In these larger systems we will place several sodium atoms between the sheets to see how two or more intercalated sodium atoms influence the energy barriers. Our results show that a sodium atom between two graphite-like molecules will be stabilized when situated between the centers of two six-membered carbon rings. The energy barriers separating these sites are considerable. Figure 7.2 shows the equilibrium bond length of sodium compared to the interstitial distances in a graphite lattice of eclipsed sheets. The potential energy curve of Na_2 is calculated with CCSD(T)/aug-cc-pVTZ and agrees well with the experimental bond length of 3.0786 Å. None of the distances a, b or c are very close to the equilibrium bond length of Na_2. This means that if two sodium atoms are placed in sites separated by a distance c, there will be repulsion, and if they are separated by distances a or b there will be attractive forces between them. This illustrates the importance of investigating a model system with several sodium atoms.
In the future, we also aim to begin investigating the interactions between sodium atoms and a graphite surface, and the penetration of sodium into the lattice. The overall goal of the DURAMAT project is to understand why sodium contamination degrades carbon materials in the cells, and thus prevent it from happening. In order to contribute to this, we must consider the carbon material surface where sodium enters. To investigate model systems large enough to describe this process, molecular mechanics (MM) methods might be required.

Charge transfer

An aspect of the sodium-graphite interactions that we have not considered in this work, is charge transfer. Graphene has a very high electron affinity ($\tilde{4}.5$ eV [42]), which means a charge transfer from sodium (which has a ionization potential of only 5.4 eV) is likely. A study by Baker and Head-Gordon [43] shows that the electron affin-

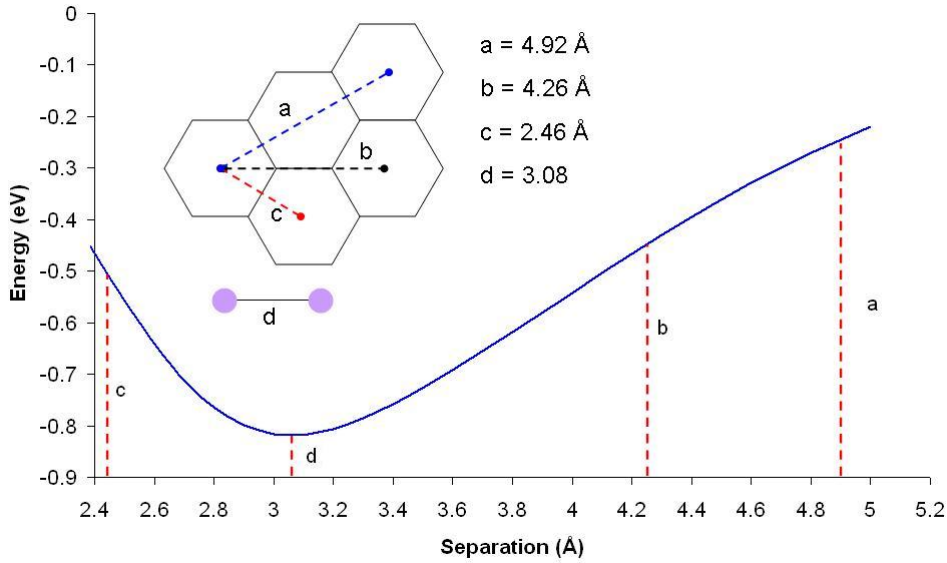

Figure 7.2: Figure 7.2 The potential energy curve of a sodium dimer calculated at the CCSD(T)/cc-pVTZ level. The distances between different sites in a graphite lattice are shown in the insert and marked on the potential energy curve. The calculated minimum corresponds well with the experimental value of 3.0786 Å

ity of polyatomic hydrocarbons (PAHs) increases with the size of the molecule. The electron affinity appears to converge towards the value of graphene as the size increases. The electron affinity of coronene is reported as approximately 0.5 eV. This highlights the need to use larger molecules (like ovalene and larger) in our calculations. In future work, we will also investigate the role of charge transfer in the interactions of sodium and graphite-like systems.

Part B

Structures and conformational energies of 1,2-dihaloethane and silane analogues

Chapter 8

Introduction

8.1 Background

Work published by Reidar Stølevik et al. [44, 45] summarizes an extensive amount of data containing structural parameters and energies of halogenated alkanes. In [44] experimental structural parameters for chloroalkanes are compared with values from molecular mechanical calculations (MM). In [45], *ab initio* calculations at the HF/6-31G* level were performed and the resulting structural energies and parameters were compared with experimental results where available. Among the molecules studied in these works, we find 1,2-difluoroethane (DFE) abd 1,2-dichloroethane (DCE). 1,2-dihaloethanes occurs in two conformers, *anti* and *gauche* (Figure 8.1). Anti and gauche isomers change into each other through a rotation around the C-C-bond, thus they are *rotomers*. The comparison of their energies has received much attention. In the context of conformational energies (i.e. the energy difference, $\Delta E = E_{anti} - E_{gauche}$), it is interesting to consider 1,2-dihaloethane substituted with all of the halogens, (F, Cl, Br and I), and their trends. In 2003, Akkerman et al. [46] presented results

from X-ray diffraction experiments on 1,2-diflouroethane (DFE) and 1,2-diiodoethane (DIE). Their results show that flourinated ethane prefers the gauche-conformation, while the iodine-species favours the anti-conformation.

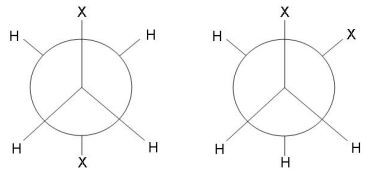

(a) Anti (b) Gauche

Figure 8.1: In the Newman projection, the difference between anti(a) and gauche(b) conformer is clearly seen.

A study by Sreeruttun and Ramasami from 2006 [47] presents experimentally and computationally determined energy differences between the anti- and gauche-conformers of 1,2-dichloroethane (DCE) and 1,2-dibromoethane (DBE). Computations were performed using MM, HF, MP2 and DFT with basis sets up to 6-311++G(d,p). All the computations indicate that both DCE and DBE favours the anti-conformation. The energy difference between the two conformations are generally more negative for bromo- than chloro-ethane.
Based on the results from literature summarized above, there appears to be a trend in the conformational energies of 1,2-dihaloethanes. For the smallest substituentt, F, gauche is the preferred conformation, while for the other three, the anti-conformation is more favourable, and the energy difference increases with the size of the substituent. This indicate that steric effects are important in determining the favoured rotomer. Thus, it is also interesting to consider the silane equivalents of the disubstituted ethane molecules, $XH_2Si\text{-}CH_2X$ and $XH_2Si\text{-}SiH_2X$ (Figure 8.2). These molecules are similar to 1,2-dihaloethanes,

although the larger silicon atoms, reduce the distance between the two halogen atoms in both anti and gauche conformations. Previous MM calculations [48] indicate that for the Si-C-species, the gauche conformer is slightly lower in energy, while for Si-Si, the gauche conformer is lower in energy by a considerable margin, the opposite of what is seen in 1,2-dihaloethanes. These results support the hypothesis that the energy difference between gauche and anti-conformers is controlled by steric repulsion between the F. However, these calculations are only performed at the MM-level and cannot be considered chemically accurate.

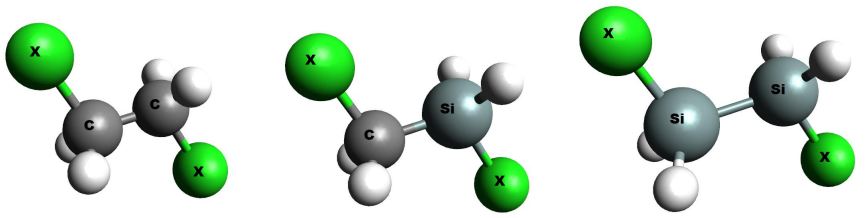

(a) 1,2-dihaloethane (b) halo(halomethyl)silane (c) 1,2-dihalodisilane

Figure 8.2: 1,2-dihaloethane and its silane analogues. Anti conformers are shown for all molecules. In this project we consider only symmetrically substituted molecules where X = F or Cl.

8.2 Nomenclature

This section describes the nomenclature we have adapted throughout this work. The molecules investigated are shown in Figure 8.2. In this figure, the molecules of type 8.2(a) are referred to by their standard IUPAC names, 1,2-di(fluoro or chloro)ethane or by the abbreviations DCE and DBE. We only consider molecules where the two

substituents are of the same type. Molecules of type 8.2(b) are referred to as fluoro(fluoromehtyl)silane and chloro(chlorometyl)silane. When referring to both these types of methylsilanes we sometimes use the term C-Si-molecules. The last type of molecules 8.2(c) are named 1,2-difluorodisilane and 1,2-dichlorodisilane, sometimes referred to as Si-Si-molecules. In this paper we sometimes use the term "silane molecules" in reference to both the latter two types of molecules.

8.3 Bond lengths

There are several definitions of bond lengths and when comparing calculations to experimental observations, it is important to distinguish between them. The symbol R_e denotes the distance between equilibrium nuclear positions; the distance between effective nuclear positions derived from rotational constants of zero-point vibrational levels are called R_0; R_g is used for the thermal average value of nuclear separation and R_α is the average internuclear distance in thermal equilibrium. The bond lengths from spectroscopic measurements are of the type R_g while those calculated in quantum chemical calculations are R_e. To compare calculated and experimental results, a conversion formula is given in [49]

$$R_g = R_e + \frac{3a_3u^2}{2} + K + \delta R \tag{8.3.1}$$

In the equation above, a_3 is the anharmonicity constant which is usually given a value of $1.5 - 2.5$ Å^{-1}. The longitudinal vibrational amplitude, u, is approximately 0.05 Å for C-C and C-Cl bonds. The perpendicular vibrations are corrected for by the term K. This constant usually takes values of 0.005 Å for C-C , 0.005-0.015 Å for C-Cl and 0.01-0.02 Å for C-H. The centrifugal distortion, δR is very small (0.001 Å) at room temperature and has been neglected. We have

Table 8.1: Corrections ($R_g - R_e$) to bond lengths from experiments

Bond	Correction ($R_g - R_e$) (Å)
C-Cl	0.010 - 0.020
C-C	0.010 - 0.015
C-H	0.02 - 0.04

adopted the same values for the corrections as in [45]. The corrections depend on the relative location of the bond in the molecule and the temperature. Therefore, each bond has been treated separately.

8.4 Goals and Hypothesis

The goal of this research is to carry out *ab initio* geometry optimizations of disubstituted ethane, methyl silane and disilane, using HF and post-HF methods with increasing accuracy. We will investigate the anti and gauche conformers of difluoro and dichloro-substituted versions of the three types of molecules shown in Figure 8.2. From geometry optimizations we will obtain structural parameters and conformational energies. For molecules where experimental results are available, a comparison between each of the methods can be made and the quality of the theoretical results can be assessed. For the silane-molecules we have not found experimental structural parameters or energies in literature. However, calculations at the CCSD(T)/cc-pVDZ level is close to the "golden standard" of computational chemistry. Bond lengths and angles from these calculations can be considered chemically accurate. The ultimate goal is to contribute to the explanation of the energy differences between anti- and gauche-conformations in disubstituted ethane and its silane analogues.

8.4.1 Overlapping work

In 2010 and 2011, two articles were published by Ramasami [50] and Ramasami et al. [51]. These works present DFT, MP2 and CCSD(T) calculations of energies and structural parameters of, among others, the silane-molecules we have investigated. The calculations were carried out using 6-311++G(d,p) and 6-311G(d,p) basis sets. They report only minor differences between the structural parameters calculated with MP2 and DFT. We discovered these articles after the work presented in this thesis was completed. The results presented in these two articles overlap with the calculations in our project. However, there are significant differences between our methods. As discussed later in Chapter 9 we use the cc-pVDZ basis set for all our geometry optimizations. In addition, Ramasami et al. have calculated geometries at the MP2 level, and then calculated energies using CCSD(T), while we have optimized all the geometries at the CCSD(T)/cc-pVDZ level. In Chapter 10 we compare our results with those from [50] and [51].

Chapter 9

Computational methods

A total of six molecules were investigated, each with two conformers, anti and gauche. The geometries of all 12 conformers were optimized using HF, MP2 and CCSD(T) with the cc-pVDZ basis set, 36 geometry optimizations in total. At the cc-pVTZ-level, these molecules are too large to conduct geometry optimizations. Rather, the optimized geometries from the cc-pVDZ calculations are used in cc-pVTZ energy calculations. The transition from double to triple zeta basis sets are kept method-specific (i.e. the optimized geometry from HF/cc-pVDZ is used in the HF/cc-pVTZ calculation, while MP2/cc-pVDZ is used for MP2/cc-pVTZ, etc). The starting points for all the geometry optimizations were HF/STO-3G-geometries from an optimization using HyperChem [52]. The geometry optimizations at the cc-pVDZ level were carried out using CFOUR [37]. Coupled cluster calculations were done using a parallel version of CFOUR [53]. The geometry optimizations are done using analytical gradients within a Quasi-Newton scheme. The convergence criteria was 10^{-5} Hartree for energies and 10^{-5} Bohr/degrees for structural parameters.

Chapter 10

Results and discussion

10.1 Conformational energies

After optimizing the geometry of both rotomers of each molecule studied, the energy differences are calculated. These are presented in Figures 10.1- 10.2. In the case of the 1,2-difluoroethane (Figure 10.1), we see that the energy difference calculated with MM is closer to the experimental value than our *ab initio* results. Among the *ab initio* calculations, there is an increase in accuracy with increasing quality of the methods. Hartree-Fock calculations predict a negative energy difference this molecule, which is wrong. For fluoro(fluoromethyl)silane and 1,2-difluorodisilane, there appears to be a trend in the energy difference with increased quality of the methods. The energy difference decreases in magnitude as the accuracy of the method increases. In fluoro(fluoromethyl)silane, the energies calculated in this study seem to converge towards the MM result with increasing quality of the method. The trend is similar for 1,2-difluorodisilane, but here, the *ab initio* results converge to almost zero (meaning the two rotomers are completely equal in energy), while MM predicts a positive energy

difference, i.e. gauche is the favoured rotomer. For these molecules we do not have experimental results, however, our calculations coincide quite well with those reported in [50] and [51]. For the two first molecules, the results match MM-calculations very well, while for the latter, MM and *ab initio* diverge.

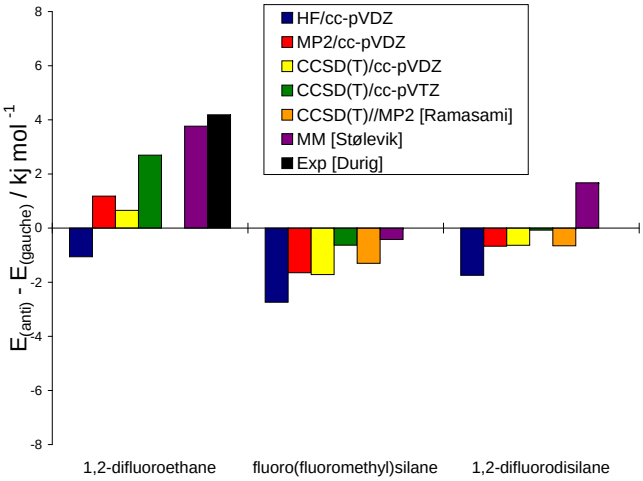

Figure 10.1: ΔE (E_{anti}-E_{gauche}) of fluorosubstitued molecules. Experimental values from Durig [54], MM results from Stølevik [48] and *ab initio* results from Ramasami et al. [50, 51] are also shown.

For 1,2-dichloroethane, we again see that the CCSD(T) results from this study coincide well with experimental results and the results from molecular mechanics calculations. However, as for DFE, the energy difference obtained from the MM calculations are closer to the experimental values than the *ab initio* results. This is surprising, since the CC-calculations should be considerably more accurate than MM. Within the CC-results for DCE, the energy calculated with

the larger basis set (triple zeta) shows an improvement with respect to the experimental result. This is as expected, since an increased basis set should give higher accuracy. In the conformational energies of chloro(chloromethyl)silane and 1,2-dichlorodisilane, we see the same distinct trend as for the fluoro-molecules in the *ab initio* calculations. The energy difference is negative for all methods, but the magnitude decreases with increased accuracy of the calculation. The MM energy difference is positive for both these molecules, and it can seem like the CCSD(T) values approach MM. However, when moving from ethane to methylsilane and then to disilane, MM predicts very large changes in the conformational energy difference. The changes in the MP2 and CCSD(T) energies are in the same direction, but a lower magnitude. This shows that the effect of replacing a carbon atom with silicon, induces the same effect in all methods. It is very likely that this is caused by reduced steric repulsion. Whatever causes this effect, it causes MM to falsely predict gauche as the conformer with the lowest energy.

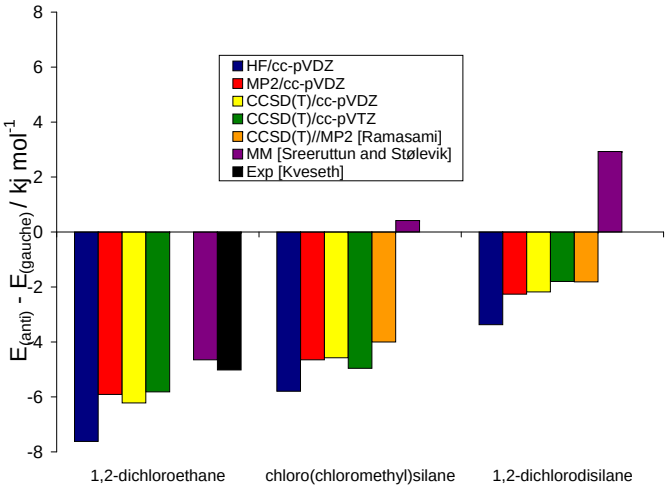

Figure 10.2: ΔE (E_{anti}-E_{gauche}) of the chlorosubstituted molecules. Experimental values from Kveseth [55], MM results from Sreeruttun et al. [47] and Stølevik [48] and *ab initio* results from Ramasami et al. [50, 51] are included in the figure

10.1.1 Conformational energy against bond lengths

When going from the ethane to methylsilane and to disilane, the bond length between the two "backbone" atoms increase. This distance is representative for the separation between the halogen substituents and thus an indicator of the repulsive forces between them. In Figure 10.3 the variation in conformational energy difference is plotted against the bond lengths (C-C, C-Si and Si-Si in Å). In the fluoro-compounds the trends in energy difference with increased "backbone" atom distance are similar for MM and CC. Both display a positive energy difference (indicating gauche is favoured) for DFE and a negative energy dif-

ference for fluoro(fluoromethyl)silane. Between these two species the trend is thus opposite to what would be expected based on steric arguments. The energy difference changes in favour of the anti-conformer with increased distance between the "backbone" atoms. This U-shaped trend is difficult to explain in terms of steric repulsion. The C-Si bond is clearly longer than the C-C distance, which should mean a shift in energy towards the gauche conformer. For both MM and CC, the energy difference shifts towards gauche when moving to the Si-Si species. Thus, the fluorosubstituted species show the same trend as the chlorines, the energy difference shifts towards gauche for the larger distance. For 1,2-difuourodisilane, the MM energy diverges from the *ab initio* results, both from this study and from [50].

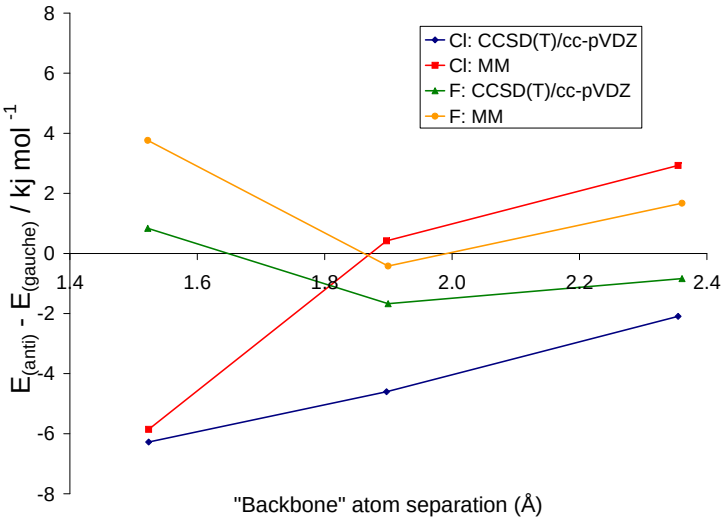

Figure 10.3: ΔE ($E_{anti} - E_{gauche}$) as a function of the distance between the "backbone" atoms (C-C, C-Si and Si-Si).

In the chlorosubstituted series, the trends in energy differences are similar between MM and CC. As the "back-bone" bond length increases, the energy difference shifts from anti towards gauche. This trend is almost linear, in contrast to the trend in the fluoro-molecules. Although the trend is very similar for MM and CCSD(T), the energy difference is negative for all molecules calculated with CCSD(T). In the MM calculations, the gauche conformer has the lowest energy for the C-Si and the Si-Si molecules. As mentioned in the previous section, the jump in the energy difference is clearly larger in MM than in CCSD(T).

10.2 Structural parameters

Experimental values of the structural parameters in DFE and DCE are available from literature. These are compared to those calculated in this study and other theoretical investigations in Tables 10.1 and 10.2. Experimental values are corrected according to Equation (8.3.1). These corrections are made in the articles we have cited. Structural parameters from experiments are only available for the lowest energy conformer. For each of the computational methods the standard deviation, with respect to the experimental bond lengths is given.

10.2.1 1,2-difluoroethane

As seen in Table 10.1 all the calculation methods overestimate the C-C bond length in DFE. It is quite surprising that the lowest level calculations (HF) gives the best values for the C-C bond length. For the C-F bond length, MP2 and CCSD(T) give values that are very close to the experimental, while HF underestimates this bond length. The standard deviation is a measure of the combined error in both bond lengths. It shows that the best correspondence with experiments is obtained in the MP2-calculations, while CCSD(T) is almost as good.

Table 10.1: Bond lengths (Å) and angles (degrees) in gauche-DFE calculated by HF, MP2 and CCSD(T). Experimental values are average of values found in [56] and [57].

	C-C	C-F	Standard deviation (Å)	C-C-F
Exp.	1.498	1.390	-	110.5
HF/6-316++G** [54]	1.503	1.365	0.018	110.5
HF/cc-pVDZ	1.501	1.367	0.016	110.3
MP2/cc-pVDZ	1.507	1.386	0.007	110.5
CCSD(T)/cc-pVDZ	1.513	1.387	0.010	110.3

When looking at the bond angle, the value from the MP2 calculations and the value from [54] are both very good, while CCSD(T) and HF values are slightly lower than the experimental.

Table 10.2: Bond lengths (Å) and angles (degrees) in anti-DCE calculated by HF, MP2 and CCSD(T. Experimental values are found in [55].

	C-C	C-Cl	Standard deviation (Å)	C-C-Cl
Exp. [55]	1.533	1.792	-	109.0
HF/6-316G* [45]	1.516	1.791	0.012	109.4
HF/cc-pVDZ	1.513	1.800	0.015	109.3
MP2/cc-pVDZ	1.518	1.791	0.010	109.3
CCSD(T)/cc-pVDZ	1.524	1.803	0.010	109.2

10.2.2 1,2-dichloroethane

In contrast to DFE, the C-C bond length is underestimated by all the calculation methods in DCE. The closest value to the experimental is

that given by CCSD(T). For the C-Cl bond, CCSD(T) overestimates the length while MP2/cc-pVDZ and HF/6-31G* is very close to the experimental value. Judging by the standard deviation, CCSD(T) coincides best with the experimental observations. In HF, the 6-31G* basis set produces results closer to the experimental values than cc-pVDZ.
In both DFE and DCE, the C-C bond length calculated by HF is shorter than that of the other two methods. In DCE, CCSD(T) provides the best prediction of the C-C bond length while in DFE, the best correspondence with experiments is actually shown by HF. These observations seem to contradict each other. It is difficult to explain exactly why MP2 and CCSD(T) both predict a longer C-C bond length than HF. Both the former methods are post-HF and include electron correlation which means they are considerably more accurate than HF. It should be noted that the gauche and anti rotamers are considered for DFE and DCE, respectively. These observations could indicate that CCSD(T) more accurately describes the anti-conformer.

10.2.3 Silane compounds

For the silane molecules investigated in this study, there are no experimental values in literature. Although the CCSD(T) and MP2 results in the section above corresponds well with experimental results, it is difficult to assess the accuracy of the calculated energies and geometries of the methylsilanes and disilanes. However, considering the high accuracy of CCSD(T)/cc-pVDZ, our results can be considered reliable. Tables with all the structural parameters from these geometry optimizations are found in Appendix B. Here, we will only discuss a few general trends from the calculations.
In the case of both 1,2-difluoro and 1,2-dichlorodisilane, the Si-Si bonds from HF calculations are longer than those from MP2 and CCSD(T). In chlorines, there is a clear trend: Si-Si$_{HF}$ > Si-Si$_{CCSD(T)}$

> Si-Si$_{MP2}$. In flourines, the MP2 and CCSD(T) Si-Si bond lengths are nearly identical, and they are both shorter than the HF bond length. This is a very different trend than in DFE and DCE, where HF predicts a shorter C-C bond.
In the flourines, the opposite trend is observed in the Si-F bond compared to the Si-Si bond. Here, HF gives a shorter bond than MP2 and CCSD(T). For 1,2-difluorodisilane, the bond lengths in the anti- and gauche-conformers are indistinguishable.
In the chloro species, the same trend is observed in the Si-Cl bonds as in the Si-Si bonds of DFE and DCE, HF bonds are longer than MP2 and CCSD(T). The Si-Si bonds are longer in gauche, while the Si-F bonds are longer in the anti conformers for all the methods.
In the methylsilane-molecules, the observed trends are quite different from those described in the disilanes. In the fluoro compounds, the C-Si, C-F and the Si-F bonds are almost identical for all methods in both anti and gauche conformers. In the chloro compounds, the trend for all bonds is bond$_{CCSD(T)}$ > bond$_{HF}$ > bond$_{MP2}$. In addition, the bond lengths are also generally longer for anti than for gauche.

10.2.4 Comparison with data from Ramasami

Bond lengths and some angles are also reported in [50, 51] for the dihalodislianes and halo(halomethyl)silanes investigated. Geometries in these studies are calculated at a MP2/6-311++G(d,p) level. The resulting bond lengths correspond very well with our values at the CCSD(T)/cc-pVDZ level. When considering all the C-Si, Si-Si, Si-X and C-X bonds in all conformers, the average deviation between the two data sets is 0.020 Å per bond. The largest deviations are found in the Si-X and C-X bonds, while the C-Si and Si-Si bonds are practically of identical length. One interesting observation is that all the bond lengths calculated with MP2 [50, 51] are shorter than those calculated with CCSD(T). There is only one exception; the C-

F bond in gauche-fluoro(fluoromethyl)silane. The bond angles of the dihalodisilanes are not reported in [50], so we will only compare angles for the halo(halomethyl)silanes. For the C-Si-X and the Si-C-X angles there is an average 0.93 degree deviation between the two data set (two angles, in both conformers of both molecules). We note that the bond angles deviate more in the anti conformers than in the gauche.

Chapter 11

Conclusion

The geometry optimizations done in this project has resulted in a large amount of data. In the previous sections we have discussed some of the results. Based on the comparison of the calculated bond lengths and angles with experimental results for DFE and DCE, it is evident that the CCSD(T)/cc-pVDZ-calculations give very accurate results. Although CCSD(T) does not give more accurate results for all bond lengths, the overall geometry is better than that calculated with HF and MP2. When comparing trends in bond lengths between computational methods and between the molecules, it is difficult to make any conclusions. While some bonds are overestimated by CCSD(T), others are overestimated by HF compared to the experimental results. A geometry optimization with CCSD(T)/cc-pVTZ would represent the "golden standard" of quantum chemistry. Although we have only used the cc-pVDZ basis sets, the results can be considered highly accurate. The experimental results referred to here, are corrected according to Equation (8.3.1). Because of the accuracy of the CCSD(T)/cc-pVDZ geometry optimizations, it becomes valid to question the parameters used in the conversion between R_g and R_e, rather than the calculated results. In order to absolutely verify this, CCSD(T)/cc-

pVTZ calculations should be performed.
The primary goal of this project was to investigate the conformational energies when moving from 1,2-dihaloethane, to halo(halomethyl)silane and then to 1,2-dihalodisilane. Previous molecular mechanics calculations report values of ΔE that predicts a shift from anti to gauche being the most stable when going from 1,2-dichloroethane to 1,2-dichlorodisilane. This does not agree with our *ab initio* calculations, although ΔE shifts *towards* gauche.
In the case of the fluorosubstituted molecules, ΔE does not follow the same trend. When going from the 1,2-dihaloethanes to the fluoro-molecule, ΔE changes from positive to negative, and then increases again in the disilane molecule. These observations indicate that the energy differences between anti and gauche-conformers are complex and cannot be explained through steric repulsion alone. The field of halo-subsituted hydrocarbons has been studied extensively, however, the highest level of *ab initio* geometry optimizations reported in literature are from MP2/6-311++G(d,p) [47, 50, 51]. The calculations in this study therefore results in an improvement in the available data. The geometries and conformational energies from our study correspond very well with results from [50] and [51] but are slightly more accurate. Comparisons with other theoretical studies are very important for molecules where experimental results are unavailable. Based on the comparison between our results and those in [50, 51] we do see that MP2 consistently overestimates the bond lengths compared to CCSD(T), but only by a margin of 0.02 Å.

Chapter 12

Future work

As mentioned in the previous chapter, CCSD(T)/cc-pVTZ geometry optimizations are the "golden standard" of quantum chemistry. We have optimized geometries at the CCSD(T)/cc-pVDZ level, and we believe that it is feasible to calculate geometries with cc-pVTZ, at least for DFE using CFOUR in parallel. These can then be compared to experimental results and will arguably be more accurate.

In this project, we have only considered fluoro- and chloro-substituted alkanes and silanes. Results have shown that there are differences in the trends in conformational energies between the two. In order to further investigate this, it would be interesting to calculate geometries of the corresponding bromo and iodo-molecules. The problem with these species, is the size of the bromine and iodine atoms. For heavy nuclei, relativistic effects begin to contribute [58]. Relativistic corrections have been developed for *ab initio* methods [59, 60] and are available in CFOUR. Geometry optimizations of the bromo-equivalents of the molecules studied here is possible, although quite costly. Bromo- and iodo-substituted molecules are included in the work by [50] and [51]. In both studies, Gaussian 03W is used. This program does include

features to correct for relativistic effects, however, they have not been used in [50, 51]. Thus, a re-calculation of the geometries in CFOUR, using the relativistic corrections available there, is an excellent opportunity to investigate the importance of these effects in iodo- and bromo-compounds and to obtain accurate energies and structural parameters to complement those from this study.

Part C

Development of ab initio computational methods based on non-orthogonal Slater determinants

Chapter 13

Background and goals

In Section 1.5 some of the most used methods in computational chemistry today were mentioned. The field of computational chemistry has made tremendous progress and the size and complexity of systems that can be investigated today are vast compared to what was possible only 20 years ago. However, much effort is still put towards the development of new methods with increased accuracy, reduced computational costs, or both. In addition, there are systems that the most common modern methods lack the ability to describe accurately, e.g Be_2. For accurate calculations of these systems, FCI is required, which is computationally very demanding. It is desirable to develop fast and accurate methods that can handle such molecules.

Koch and Dalgaard [61] present an alternative multiconfigurational-SCF (MCSCF) approach. In contrast to common practice, their proposed method does not place requirements of orthogonality on the determinants used. This results in a much more flexible wave function, but decreases the computational speed. In order to save time, an alternative optimization procedure is also suggested. The method uses the HF wave function as a starting point. Determinants are added to

this reference and optimized one at a time.
The method has been shown to give a near full-CI description of the electron correlation energy of simple systems, using much fewer determinants than what is needed in other MCSCF-methods. In [61], the method was tested, and showed good results for a water molecule in its equilibrium geometry, a Be-atom and for the BH-molecule. The quality of the calculations was measured in percentage of electron correlation recovered. For Be, 92.2% of the electron correlation was obtained by using ten determinants, and 99.9% was achieved with 120 determinants. For water, 88.8% was recovered by adding ten determinants, and 99.5% from 160 determinants. The non-orthogonal Slater-determinant (NOSD) method can in the future be combined with coupled cluster such that the orbitals in the cluster operator are non-orthogonal to the orbitals in the reference determinant. This will allow the description of chemical reactions using CC-methods [62]. When the code was tested in 1993, it was programmed in a free-standing program which is not very practical. Implementation of the method in Dalton is the first step towards a combination of NOSD with CC. The objective of this part of the thesis, is to present the theoretical background of the method in a clear manner and to implement and test the method in Dalton [63] for singlet systems.

13.1 Test systems

After implementing the NOSD code in Dalton we wish to test its performance. We are particularly interested in the amount of electron correlation energy recovered, its computational speed and if it is able to describe systems where other common methods (MP2, CCSD and CCSD(T)) fail. We have chosen to test the NOSD code on water and the beryllium dimer. Binding and absolute energies from our calculations will be compared to experimental and theoretical results

from literature.

13.1.1 Water

In [64], results from calculations using various methods on water in its equilibrium geometry and during symmetric stretching of the O-H bonds is presented. Among the methods tested are MP2 and CCSD(T), along with higher level calculations with both MBPT and CC. The higher level methods (e.g. MP15 and CCSDTQ) produce very accurate results, but similar to FCI calculations, these are very costly. Our goal is for NOSD to be a method that can produce accurate results in a relatively short time. We will therefore focus on the comparison of our results to those from MP2 and CCSD(T).

13.1.2 Be_2

The beryllium dimer, Be_2, is an enigma for computational chemistry, despite its modest size (8 electrons). Early theoretical studies using both SCF [65, 66] and CI [67] concluded that the dimer was completely repulsive. Since then, different studies have presented results varying from a shallow van der Waals minima to double minima and bond lengths between 2.3 and 5.1 Å. In 2007, a study by Patkowski et al. [68] presented the full configuration interaction (FCI) binding energy for Be_2. The calculations were conducted by first calculating the CCSD(T)-energy, extrapolating this to the complete basis set limit (CBS) and then doing a FCI-calculation within the frozen core (FC) approximation. The resulting binding energy was 938 cm^{-1} at a fixed bond length of 2.44 Å. In 2009, a spectroscopic study by Merritt et al. [69] presented an experimental well depth and bond lengths of 929.742 cm^{-1} and 2.45 Å, respectively. This coincides very well with the theoretical results from Patkowski and it appears that the correct bond length and binding energy has been found. The method

employed by Patkowski is computationally very demanding, however, none of the faster methods (MP2, CCSD or CCSD(T)) produce accurate results. Our goal is to use NOSD to obtain an accurate description of Be_2.

Chapter 14

Theory

In this chapter we will go through the derivation of the equations that form the theoretical basis for the method based on non-orthogonal Slater determinants (NOSD). Chapter 15 will describe the implementation of the method in Dalton.

14.1 Matrix elements

The state of a system is described by a wave function that can be written as a linear combination of Slater determinants

$$|\Psi\rangle = \sum_j |\phi_j\rangle \, C_j \tag{14.1.1}$$

We start with a primitive basis of M orthonormal spin-orbitals $\{ \omega_q(\xi) \}$ and their corresponding creation operators $\{ a_q^\dagger \}$. In this basis, the Hamiltonian is given by

$$H = \sum_{p,q} h_{pq} a_p^\dagger a_q + \tfrac{1}{2} \sum_{p,r,q,s} (pq|rs) \, a_p^\dagger a_r^\dagger a_s a_q \tag{14.1.2}$$

We will assume that the one- and two-electron integrals in this basis are known. Let us then imagine that one of the determinants in the expansion in Equation (14.1.1) is given by

$$|\phi\rangle = b_1^\dagger b_2^\dagger \dots b_n^\dagger \,|\text{vac}\rangle \tag{14.1.3}$$

Where, $\left\{ b_j^\dagger \right\}$ are the creation operators for the spin orbitals $\{ \nu_q(\xi) \}$ that are occupied in ϕ. These spin orbitals can be expressed as a linear combination of the spin orbitals in the original orthonormal basis $\{ \omega_q(\xi) \}$

$$\nu_j = \sum_p \omega_p D_{pj}(\phi) \tag{14.1.4}$$

Here $\mathbf{D}(\phi)$ is a rectangular $M \times n$ matrix. Similarly, the creation operators in this basis can be expressed as a linear combinations of the original creation operators

$$b_p^\dagger = \sum_r a_r^\dagger D_{rp}(\phi) \tag{14.1.5}$$

The objective is now to describe the matrix elements required to calculate the electronic energy using arbitrary, not necessarily orthogonal Slater determinants. The simplest matrix element is the scalar product $\langle\phi'|\phi\rangle$ where ϕ is given as above and where ϕ' is a different determinant with occupied orbitals $\{ u_q(\xi) \}$ given by

$$u_j = \sum_p \omega_p D_{pj}(\phi') \tag{14.1.6}$$

and the corresponding creation operators $\left\{ c_j^\dagger \right\}$ are given as

$$c_p^\dagger = \sum_r a_r^\dagger D_{rp}(\phi') \tag{14.1.7}$$

The scalar product between these two determinants can be expressed as the determinant of an overlap matrix Δ

$$\langle \phi' \,|\, \phi \rangle = |\Delta| \tag{14.1.8}$$

The equation above can be shown using the anti-commutator relations of the creation operators.

$$\begin{aligned}
\left[c_p, b_q^\dagger\right]_+ &= \sum_{r,s} \left[a_r D_{rp}^*(\phi'), a_s^\dagger D_{sq}(\phi)\right]_+ \\
&= \sum_{r,s} D_{rp}^*(\phi') \delta_{rs} D_{sq}(\phi) \\
&= \sum_{r} D_{rp}^*(\phi') D_{rq}(\phi) \\
&= \langle u_p \,|\, \nu_q \rangle
\end{aligned} \tag{14.1.9}$$

Equation (14.1.8) holds for determinants of any length. Below, the equation is derived for two two-electron determinants. The vacuum state is usually denoted $|\text{vac}\rangle$. We introduce the notation $\langle x \rangle$ for the vacuum expectation value of the operator x. We can rewrite the scalar product of any two determinants by "moving" the annihilation operators from left to right by inserting relation for the anti-commutators.

$$
\begin{aligned}
\langle \phi' \,|\, \phi \rangle &= \left\langle c_2 c_1 b_1^\dagger b_2^\dagger \right\rangle \\
&= \left\langle c_2 \left(c_1 b_1^\dagger + b_1^\dagger c_1 - b_1^\dagger c_1 \right) b_2^\dagger \right\rangle \\
&= \left\langle c_2 \left(\left[c_1, b_1^\dagger \right]_+ - b_1^\dagger c_1 \right) b_2^\dagger \right\rangle \\
&= \left\langle c_2 \left[c_1, b_1^\dagger \right]_+ b_2^\dagger \right\rangle - \left\langle c_2 b_1^\dagger c_1 b_2^\dagger \right\rangle \\
&= \left[c_1, b_1^\dagger \right]_+ \left\langle c_2 b_2^\dagger \right\rangle - \left(\left[c_1, b_2^\dagger \right]_+ \left\langle c_2 b_1^\dagger \right\rangle - \left\langle c_2 b_1^\dagger b_2^\dagger c_1 \right\rangle \right) \\
&= \left[c_1, b_1^\dagger \right]_+ \left\langle c_2 b_2^\dagger \right\rangle - \left[c_1, b_2^\dagger \right]_+ \left\langle c_2 b_1^\dagger \right\rangle
\end{aligned}
$$

After moving all annihilation operators to the right we are left with

$$
\begin{aligned}
\langle \phi' \,|\, \phi \rangle &= \left[c_1, b_1^\dagger \right]_+ \left[c_2, b_2^\dagger \right]_+ - \left[c_1, b_2^\dagger \right]_+ \left[c_2, b_1^\dagger \right]_+ \\
&= \langle u_1 \,|\, \nu_1 \rangle \langle u_2 \,|\, \nu_2 \rangle - \langle u_1 \,|\, \nu_2 \rangle \langle u_2 \,|\, \nu_1 \rangle = |\Delta| \qquad (14.1.10)
\end{aligned}
$$

The matrix element arising from the one-electron term of the Hamiltonian can be calculated in a similar fashion

$$
\begin{aligned}
\left\langle \phi' \,\middle|\, a_p^\dagger a_q \,\middle|\, \phi \right\rangle &= \left\langle \phi' \,\middle|\, \left[a_p^\dagger, a_q \right]_+ \,\middle|\, \phi \right\rangle - \left\langle \phi' \,\middle|\, a_q a_p^\dagger \,\middle|\, \phi \right\rangle \qquad (14.1.11) \\
&= \delta_{pq} \langle \phi' \,|\, \phi \rangle - \left\langle \phi' \,\middle|\, a_q a_p^\dagger \,\middle|\, \phi \right\rangle \qquad (14.1.12)
\end{aligned}
$$

The second term in the last line is equivalent to the determinant of a $n+1$ electron determinant overlap and can be expanded as in the derivation above.

$$\begin{aligned}
\left\langle \phi' \,\middle|\, a_p^\dagger a_q \,\middle|\, \phi \right\rangle &= \delta_{pq} \left\langle \phi' \,|\, \phi \right\rangle - \left\langle \phi' \,\middle|\, a_q a_p^\dagger \,\middle|\, \phi \right\rangle \\
&= \delta_{pq}|\Delta| - \det \begin{pmatrix} \delta_{qp} & \left\langle a_q b_1^\dagger \right\rangle & \left\langle a_q b_2^\dagger \right\rangle & \dots & \left\langle a_q b_n^\dagger \right\rangle \\ \left\langle c_1 a_p^\dagger \right\rangle & & & & \\ \left\langle c_2 a_p^\dagger \right\rangle & & \Delta & & \\ \vdots & & & & \\ \left\langle c_n a_p^\dagger \right\rangle & & & & \end{pmatrix} \\
&= -\det \begin{pmatrix} 0 & \left\langle a_q b_1^\dagger \right\rangle & \left\langle a_q b_2^\dagger \right\rangle & \dots & \left\langle a_q b_n^\dagger \right\rangle \\ \left\langle c_1 a_p^\dagger \right\rangle & & & & \\ \left\langle c_2 a_p^\dagger \right\rangle & & \Delta & & \\ \vdots & & & & \\ \left\langle c_n a_p^\dagger \right\rangle & & & & \end{pmatrix}
\end{aligned} \tag{14.1.13}$$

We are thus left with a single determinant of a $(n+1)\times(n+1)$ matrix. To simplify the expression above, we use the relation

$$\det \begin{pmatrix} A & B \\ C & D \end{pmatrix} = \det\mathbf{D} \times \det\left(\mathbf{A} - \mathbf{B}\mathbf{D}^{-1}\mathbf{C}\right) \tag{14.1.14}$$

Applying this to the last line of Equation (14.1.13) we obtain an expression for the one electron integral in terms of the $\mathbf{D}$ matrixes from equations (14.1.4) and (14.1.6)

$$\begin{aligned}
\left\langle \phi' \,\middle|\, a_p^\dagger a_q \,\middle|\, \phi \right\rangle &= -|\Delta| \times \det\left(-\left\langle a_q b_\mu^\dagger \right\rangle (\Delta)^{-1}_{\mu\nu} \left\langle c_\nu a_p^\dagger \right\rangle\right) \\
&= |\Delta| \times \det\left(D_{q\mu}(\phi)(\Delta)^{-1}_{\mu\nu} D^*_{\nu p}(\phi')\right) \\
&= |\Delta| \times \left[\mathbf{D}(\phi)(\Delta)^{-1}_{\mu\nu}\mathbf{D}(\phi')^\dagger\right]_{qp} \equiv g_{qp}
\end{aligned} \tag{14.1.15}$$

The next step is to evaluate the two-electron integrals. Using the same approach, introducing the anti-commutators by moving annihilation operators towards the *ket*, we find that the two electron density matrix is given by

$$\left\langle \phi' \,\middle|\, a_p^\dagger a_r^\dagger a_s a_q \,\middle|\, \phi \right\rangle = (g_{qp}g_{sr} - g_{sp}g_{qr})|\Delta|^{-1} \tag{14.1.16}$$

This expression becomes unstable when the determinant of the overlap matrix is close to zero. To avoid this problem we introduce a singular value decomposition of the overlap matrix

$$\Delta = \mathbf{UdV}^+ \tag{14.1.17}$$

Where $\mathbf{U}$ and $\mathbf{V}$ are unitary matrices with determinants equal to one and $\mathbf{d}$ is a diagonal matrix. The determinant of a product of matrixes equals to product of the determinants. The determinant of a diagonal matrix is the product of all the diagonal elements, so the scalar product of two determinants can then be written as

$$\langle \phi' \,|\, \phi \rangle = \prod_j d_j \tag{14.1.18}$$

where d_j are the elements of d. Using this alternative formulation of the overlap matrix, the one- and two-electron densities can be rewritten. The one electron matrix element is then given by

$$g_{qp} = \left[\mathbf{D}(\phi)\mathbf{V}\mathbf{p}\mathbf{U}^+\mathbf{D}(\phi')^\dagger\right]_{qp} \tag{14.1.19}$$

where $\mathbf{p}$ is a diagonal matrix with elements $p_j = d_1 d_2 \ldots d_{j-1} d_{j+1} \ldots d_n$. In order to simplify the two-electron matrix elements we introduce the quantity $f(qp, jj')$

$$f(qp, jj') = \left(\mathbf{D}(\phi)\mathbf{V}\right)_{qj} \left(\mathbf{D}(\phi')\mathbf{U}\right)^*_{pj'} \tag{14.1.20}$$

The two-electron elements can then be rewritten to a more stable form. We begin by considering the first term on the right hand side of Equation (14.1.16)

$$
\begin{aligned}
g_{qp}g_{sr}|\Delta|^{-1} &= \left[\mathbf{D}(\phi)\mathbf{V}\mathbf{d}^{-1}\mathbf{U}^{+}\mathbf{D}(\phi')^{\dagger}\right]_{qp} \times \\
&\quad \left[\mathbf{D}(\phi)\mathbf{V}\mathbf{d}^{-1}\mathbf{U}^{+}\mathbf{D}(\phi')^{\dagger}\right]_{sr}|\Delta| && (14.1.21)\\
&= \sum_{jj'} (\mathbf{D}(\phi)\mathbf{V})_{qj} d_j^{-1} (\mathbf{U}^{+}\mathbf{D}(\phi')^{+})_{jp} \\
&\quad (\mathbf{D}(\phi)\mathbf{V})_{sj'} d_{j'}^{-1} (\mathbf{U}^{+}\mathbf{D}(\phi')^{+})_{j'r}|\Delta| && (14.1.22)\\
&= \sum_{jj'} (\mathbf{D}(\phi)\mathbf{V})_{qj} (\mathbf{D}(\phi')\mathbf{U})^{*}_{pj} \\
&\quad (\mathbf{D}(\phi)\mathbf{V})_{sj'} (\mathbf{D}(\phi')\mathbf{U})^{*}_{j'r} d_j^{-1} d_{j'}^{-1}|\Delta| && (14.1.23)\\
&= \sum_{jj'} f(qp,jj) f(sr,j'j') d_j^{-1} d_{j'}^{-1}|\Delta| && (14.1.24)
\end{aligned}
$$

Replacing both terms in Equation (14.1.16) as shown above yields

$$
\begin{aligned}
\left\langle \phi' \,\middle|\, a_p^{\dagger} a_r^{\dagger} a_s a_q \,\middle|\, \phi \right\rangle &= \sum_{jj'} f(qp,jj) f(sr,j'j') d_j^{-1} d_{j'}^{-1}|\Delta| \\
&\quad - \sum_{jj'} f(qp,jj') f(sr,jj') d_j^{-1} d_{j'}^{-1}|\Delta| && (14.1.25)
\end{aligned}
$$

This can be simplified further by introducing the definition

$$
d_j^{-1} d_{j'}^{-1}|\Delta| = \prod_{q \neq j,j'} d_q = q_{jj'} \tag{14.1.26}
$$

Which leaves us with

$$\left\langle \phi' \,\middle|\, a_p^\dagger a_r^\dagger a_s a_q \,\middle|\, \phi \right\rangle = \sum_{jj'} [f(qp,jj)f(sr,j'j') - f(qp,jj')f(sr,jj')]q_{jj'} \tag{14.1.27}$$

Using the equations in this section, the matrix elements needed to calculate the energy of a general spin-orbital basis can be found. In the rest of the equations and throughout this thesis, the focus will be on singlet states with $2n$ electrons. The orbital indices $i, j, k, \ldots$ will refer to occupied spatial orbitals and the indices $a, b, c, \ldots$ will indicate virtual orbitals. All determinants will contain an equal number of orbitals with α and β spin, with identical spatial parts. We will use the modified defintions

$$|\Delta| = \langle \phi'_\alpha | \phi_\alpha \rangle \tag{14.1.28}$$

$$g_{qp} = \langle \phi'_\alpha | a_{p\alpha}^\dagger a_{q\alpha} | \phi_\alpha \rangle \tag{14.1.29}$$

This gives the following expression for the total energy of a singlet state

$$\begin{aligned}
\langle\phi'|H|\phi\rangle = &\langle\phi'_\beta\phi'_\alpha|\sum_{p,q} h_{rs}\left(a^\dagger_{p\alpha}a_{q\alpha} + a^\dagger_{p\beta}a_{q\beta}\right)|\phi_\alpha\phi_\beta\rangle \\
&+ \langle\phi'_\beta\phi'_\alpha|\left[\frac{1}{2}\sum_{p,q,r,s}(pq|rs)\left(a^\dagger_{p\alpha}a^\dagger_{r\alpha}a_{s\alpha}a_{q\alpha}\right)\right]|\phi_\alpha\phi_\beta\rangle \\
&+ \langle\phi'_\beta\phi'_\alpha|\left[\frac{1}{2}\sum_{p,q,r,s}(pq|rs)\left(a^\dagger_{p\beta}a^\dagger_{r\beta}a_{s\beta}a_{q\beta}\right)\right]|\phi_\alpha\phi_\beta\rangle \\
&+ \langle\phi'_\beta\phi'_\alpha|\left[\frac{1}{2}\sum_{p,q,r,s}(pq|rs)\left(a^\dagger_{p\alpha}a^\dagger_{r\beta}a_{s\beta}a_{q\alpha}\right)\right]|\phi_\alpha\phi_\beta\rangle \\
&+ \langle\phi'_\beta\phi'_\alpha|\left[\frac{1}{2}\sum_{p,q,r,s}(pq|rs)\left(a^\dagger_{p\beta}a^\dagger_{r\alpha}a_{s\alpha}a_{q\beta}\right)\right]|\phi_\alpha\phi_\beta\rangle \qquad (14.1.30)
\end{aligned}$$

The first term in Equation (14.1.30) is the one-electron contribution which can be simplified to

$$\begin{aligned}
&\langle\phi'_\beta\phi'_\alpha|\sum_{p,q} h_{rs}\left(a^\dagger_{p\alpha}a_{q\alpha} + a^\dagger_{p\beta}a_{q\beta}\right)|\phi_\alpha\phi_\beta\rangle \\
&= \sum_{p,q} h_{rs}\left(\langle\phi'_\beta|\phi_\beta\rangle\langle\phi'_\alpha|a^\dagger_{p\alpha}a_{q\alpha}|\phi_\alpha\rangle + \langle\phi'_\alpha|\phi_\alpha\rangle\langle\phi_\beta|a^\dagger_{p\beta}a_{q\beta}|\phi_\beta\rangle\right) \\
&= \sum_{pq} h_{pq}\left(|\Delta|g_{qp} + |\Delta|g_{qp}\right) \\
&= 2|\Delta|\sum_{pq} h_{pq}g_{qp} \qquad (14.1.31)
\end{aligned}$$

The four last terms in Equation (14.1.30) are the two-electron contributions. They can be simplified according to the derivation below

$$
\begin{aligned}
&\frac{1}{2}\sum_{p,q,r,s}(pq|rs) \\
&\langle\phi'_\alpha|\left(a^\dagger_{p\alpha}a^\dagger_{r\alpha}a_{s\alpha}a_{q\alpha}\right)|\phi_\alpha\rangle\,\langle\phi'_\beta|\phi_\beta\rangle \\
&+\langle\phi'_\beta|\left(a^\dagger_{p\beta}a^\dagger_{r\beta}a_{s\beta}a_{q\beta}\right)|\phi_\beta\rangle\,\langle\phi'_\alpha|\phi_\alpha\rangle \\
&+\langle\phi'_\alpha|\left(a^\dagger_{p\alpha}a_{q\alpha}\right)|\phi_\alpha\rangle\,\langle\phi'_\beta|a^\dagger_{r\beta}a_{s\beta}|\phi_\beta\rangle \\
&+\langle\phi'_\alpha|\left(a^\dagger_{r\alpha}a_{s\alpha}\right)|\phi_\alpha\rangle\,\langle\phi'_\beta|a^\dagger_{p\beta}a_{q\beta}|\phi_\beta\rangle \\
&=\frac{1}{2}\sum_{p,q,r,s}(pq|rs)\left[2\left(g_{qp}g_{sr}-g_{sp}g_{qr}\right)+2g_{qp}g_{sr}\right] \\
&=\sum_{p,q,r,s}2\,(pq|rs)\,g_{qp}g_{sr}-(pq|rs)\,g_{sp}g_{qr} \\
&=\sum_{p,q,r,s}2\,(pq|rs)\,g_{qp}g_{sr}-(ps|rq)\,g_{qp}g_{sr} \\
&=\sum_{p,q,r,s}\left[2\,(qp|rs)-(ps|rq)\right]g_{qp}g_{sr} \\
&=\sum_{p,q,r,s}M(pq,rs)g_{qp}g_{sr}
\end{aligned}
\tag{14.1.32}
$$

Where we have introduced the definition

$$M(pq,rs)\equiv 2\,(qp|rs)-(ps|rq) \tag{14.1.33}$$

Combining the results from Equations (14.1.31) and (14.1.32) we can write the total Hamiltonian matrix element of a singlet state as

$$\langle\phi'|H|\phi\rangle = 2|\Delta|\sum_{pq}h_{pq}g_{qp}+\sum_{p,q,r,s}M(pq,rs)g_{qp}g_{sr} \tag{14.1.34}$$

The matrix elements of the Hamiltonian is used for the calculation of the energy. Recalling that the energy is given by

$$E = \frac{\langle \Psi | H | \Psi \rangle}{\langle \Psi | \Psi \rangle} \tag{14.1.35}$$

Here, we can insert a linear combination of non-orthogonal Slater determinants which yields

$$E = \frac{\sum_{IJ} C_I \langle \phi_I | H | \phi_J \rangle C_J}{\sum_{IJ} C_I \langle \phi_J | \phi_I \rangle C_I} \tag{14.1.36}$$

Where the matrix elements are given by Equations (14.1.34) and (14.1.10).

14.2 Orbital parameterization

The topic of orbital rotations was discussed in Section 1.4. We use this type of rotations in order to generate new determinants form a reference determinant (usually the Hartree-Fock wave function).

$$|\phi\rangle = \exp(i\Lambda) |R\rangle \tag{14.2.1}$$

Here, Λ is a Hermitian one-particle operator of rank zero with respect to spin-rotations. For real orbitals, Λ is written as

$$\Lambda = -i \sum_{b,j} \left(a^\dagger_{b\alpha} a_{j\alpha} - a^\dagger_{j\alpha} a_{b\alpha} + a^\dagger_{b\beta} a_{j\beta} - a^\dagger_{j\beta} a_{b\beta} \right) \lambda_{bj} \tag{14.2.2}$$

Using this rotation on a determinant, creates a matrix $\mathbf{D}$ (Equation (14.1.4)), which depends on the parameters λ_{bj} in a quite complicated way. The matrix λ is rectangular and the first index a runs over all the virtual orbitals $(a, b, c, \ldots)$ while the second index denotes the occupied orbitals $(i, j, k, \ldots)$. In order to simplify the expression for $\mathbf{D}$ we suggest an SVD of λ.

$$\lambda_{bj} = \sum_{p} A_{bp} \theta_p B_{jp} \tag{14.2.3}$$

Above, $\mathbf{A}$ and $\mathbf{B}$ are real, orthogonal matrixes of dimensions $M-n$ and n respectively. The diagonal matrix θ has at most n non-zero elements and $\theta_p = 0$ when $p > n$. Using this SVD we can derive expressions for the unitary orbital transformations generated by Λ. Let us first consider the transformation of the virtual spin orbitals of the reference state, $|R\rangle$. In the singlet state case we begin with considering only the α-terms in Equation (14.2.2). From Equation (1.4.8) we see that

$$\begin{aligned} \exp(\imath\Lambda^\alpha) a^\dagger_{a\alpha} \exp(-\imath\Lambda^\alpha) &= \tilde{a}^\dagger_{a\alpha} \\ &= a^\dagger_{a\alpha} + \left[\Lambda^\alpha, a^\dagger_{a\alpha}\right] + \tfrac{1}{2}\left[\Lambda^\alpha, \left[\Lambda^\alpha, a^\dagger_{a\alpha}\right]\right] + \ldots \end{aligned} \tag{14.2.4}$$

If the series is truncated at after the third term we need to calculate two determinants. From this point forward, we assume that we are dealing with the α-contribution and omit the subscript for clarity. Using the single value decomposition of λ_{bj} the commutator in the second term on the right hand side of Equation (14.2.4) is equal to

$$\begin{aligned}
\left[\Lambda, a_a^\dagger\right] &= \left[\left(\sum_{b,j} a_b^\dagger a_j - a_j^\dagger a_b \sum_p A_{bp}\theta_p B_{jp}\right), a_a^\dagger\right] \\
&= \sum_{b,j,p}\left(\left[a_b^\dagger a_j, a_a^\dagger\right] - \left[a_j^\dagger a_b, a_a^\dagger\right]\right) A_{bp}\theta_p B_{jp} \qquad (14.2.5)
\end{aligned}$$

$$\begin{aligned}
\left[a_b^\dagger a_j, a_a^\dagger\right] &= a_b^\dagger \delta_{ja} = 0 \\
\left[a_j^\dagger a_b, a_a^\dagger\right] &= a_j^\dagger \delta_{ab} \\
\left[\Lambda, a_a^\dagger\right] &= -\sum_{b,j,p} a_j^\dagger \delta_{ab} A_{bp}\theta_p B_{jp} \\
&= -\sum_{j,p} a_j^\dagger A_{ap}\theta_p B_{jp} \qquad (14.2.6)
\end{aligned}$$

Which can be rearranged to

$$\left[\Lambda, a_a^\dagger\right] = -\sum_{j,p} a_j^\dagger B_{jp}\theta_p \left(A_{pa}\right)^T = -\sum_j a_j^\dagger \left[B\theta A^T\right]_{ja} \qquad (14.2.7)$$

Inserting the result from above into the commutator in the third term on the right side in Equation (14.2.4) we obtain in a similar way

$$\begin{aligned}
\left[\Lambda, \left[\Lambda, a_a^\dagger\right]\right] &= -\left[\left(\sum_{b,j,p}\left(a_b^\dagger a_j - a_j^\dagger a_b\right) A_{bp}\theta_p B_{jp}\right), \sum_{i,q} a_i^\dagger A_{aq}\theta_q B_{iq}\right] \\
&= -\sum_{b,j,i,p,q}\left(\left[a_b^\dagger a_j, a_i^\dagger\right] - \left[a_j^\dagger a_b, a_i^\dagger\right]\right) A_{bp}\theta_p B_{jp} A_{aq}\theta_q B_{iq} \\
&= -\sum_{b,j,i,p,q}\left(a_b^\dagger \delta_{ji} - a_j^\dagger \delta_{bi}\right) A_{bp}\theta_p B_{jp} A_{aq}\theta_q B_{iq} \\
&= -\sum_{b,j,p,q} a_b^\dagger A_{bp}\theta_p \theta_q A_{aq} B_{jp} B_{jq} \qquad (14.2.8)
\end{aligned}$$

By noting that

$$B_{jp}B_{jq} = \delta_{pq} \tag{14.2.9}$$

Equation (14.2.8) reduces to

$$\left[\Lambda, \left[\Lambda, a_a^\dagger\right]\right] = -\sum_{b,p} a_b^\dagger A_{bp}\theta_p\theta_p A_{ap} \tag{14.2.10}$$

Similarly to what was done in the first commutator term, we can write this as

$$\left[\Lambda, \left[\Lambda, a_a^\dagger\right]\right] = -\sum_{b,p} a_b^\dagger A_{bp}\theta_p\theta_p A_{ap} = -\sum_{b} a_b^\dagger \left[A\theta^2 A^T\right]_{ba} \tag{14.2.11}$$

Inserting the results from the two previous expressions into Equation (14.2.4) we obtain

$$\tilde{a}_a^\dagger = a_{a\alpha}^\dagger - \sum_{j,p} a_j^\dagger A_{ap}\theta_p B_{jp} - \tfrac{1}{2}\sum_{b,p} a_b^\dagger A_{bp}\theta_p\theta_p A_{ap}\ldots \tag{14.2.12}$$

Let us now compare the terms in series in Equation (14.2.12) to the Taylor series expansion of the sine and cosine functions

$$\sin\theta = 1 - \frac{\theta^2}{2!} + \frac{\theta^4}{4!} - \ldots \tag{14.2.13}$$

$$\cos\theta = \theta - \frac{\theta^3}{3!} + \frac{\theta^5}{5!} - \ldots \tag{14.2.14}$$

Using the Taylor series expansions, Equation (14.2.12) can be rewritten in terms of the trigonometric functions to form

$$\tilde{a}_a^\dagger = \sum_{b} a_b^\dagger \left[A\cos\theta A^T\right]_{ba} - \sum_{j} a_j^\dagger \left[B\sin\theta A^T\right]_{ja} \tag{14.2.15}$$

Using the same approach we can write a similar expression for the occupied spin-orbitals in the reference state

$$\tilde{a}_i^\dagger = \sum_a a_b^\dagger \left[A \sin\theta B^T\right]_{ai} + \sum_j a_j^\dagger \left[B \cos\theta B^T\right]_{ji} \tag{14.2.16}$$

In Equations (14.2.15) and (14.2.16), the transposed matrixes $\mathbf{A}^T$ and $\mathbf{B}^T$, respectively, can be factorized out of the two terms. The multiplication of these matrices represent unitary transformations of the orbitals and is thus irrelevant for the energy. Therefore, we can write the occupied spin orbitals as

$$\begin{aligned} \nu_p(\mathbf{r}) &= \sum_a \omega_a A_{ap} \sin\theta_p + \sum_j \omega_j B_{jp} \cos\theta_p \\ &\equiv \sum_s \omega_s D(\phi)_{sp} \end{aligned} \tag{14.2.17}$$

where $p = 1, 2, \ldots, n$. A similar expression can be written for the virtual orbitals.

$$\begin{aligned} w_p(\mathbf{r}) &= \sum_b \omega_b A_{bp} \cos\theta_p - \sum_i \omega_i B_{ip} \sin\theta_p \\ &\equiv \sum_s \omega_s Q(\phi)_{sp} \end{aligned} \tag{14.2.18}$$

where $p = 1, 2, \ldots, M - n$

14.3 Initial guess

An underlying principle in this method is to improve the energy by sequentially adding determinants to the wave function in order to improve the energy. Imagine a reference wave function, e.g. the HF state, being improved by adding an additional Slater determinant

$$|\Psi\rangle = |\Psi_0\rangle\, C_0 + |\phi\rangle\, C_1 \tag{14.3.1}$$

In the suggested approach, each optimization is initiated by adding the previously optimized determinant as input. This will not lead to a change in the energy. From the variational principle equation below holds

$$E = \frac{\langle\Psi|H|\Psi\rangle}{\langle\Psi|\Psi\rangle} \geq \varepsilon_0 \tag{14.3.2}$$

Where, ε_0 is the experimental ground state energy. The coefficients C_0 and C_1 are then variational parameters of the total wave function and the gradient with respect to C_1 can be written as

$$\frac{\partial E}{\partial C_1} = \frac{\frac{\partial}{\partial C_1}\langle\Psi|H|\Psi\rangle}{\langle\Psi|\Psi\rangle} - \frac{\langle\Psi|H|\Psi\rangle}{\langle\Psi|\Psi\rangle^2}\frac{\partial}{\partial C_1}\langle\Psi|\Psi\rangle = 0 \tag{14.3.3}$$

To simplify the notation, we will from now on assume that the wave function is normalized. The condition for the energy to be stationary is that

$$\frac{\partial E}{\partial C_1} = 2\big(\langle\Psi|H|\phi_1\rangle - E\langle\Psi|\phi_1\rangle\big) = 0 \tag{14.3.4}$$

And similarly for C_0. This leads to the familiar equation

$$(\mathbf{H} - \mathbf{S}E)\,\vec{C} = \vec{0} \tag{14.3.5}$$

$$\Leftrightarrow |\mathbf{H} - \mathbf{S}E| = 0 \tag{14.3.6}$$

In Section 1.4 we describe the concept of unitary orbital transformations using an exponential operator. Let us imagine that the Slater determinant added in Equation (14.3.1) is expressed as a transformation of a reference determinant, $|\phi\rangle = \exp(\imath\Lambda)\,|R\rangle$.

$$|\Psi\rangle = |\Psi_0\rangle\, C_0 + \exp(\imath\Lambda)\, |R\rangle\, C_1 \tag{14.3.7}$$

The wave function still obeys the variational principle, and since the rotation depends on the parameters $\{\lambda_{bj}\}$ (Equation (14.2.3)), these are now also variational parameters. Thus we can write

$$\frac{\partial E}{\partial \lambda_{bj}} = 2C\, \langle \Psi | H - E | \tfrac{\partial \phi}{\partial \lambda_{bj}} \rangle \tag{14.3.8}$$

This will also vanish since we are at a minimum in the energy. In order to optimize the new wave function, a modification of the variables $\{\lambda_{bj}\}$ has to be made. A rigorous procedure for this modification is not yet developed, but a temporary solution has proved successful. In coupled cluster calculations, the wave function is improved by adding states corresponding to e excitations. We adopt a similar approach. Adding a determinant that corresponds to a single excitation from HOMO, ϕ_j, to LUMO, ϕ_a, would be similar to the approach in CCS. However, we do not impose orthogonality, and the added determinant does not have to be one where an electron is completely excited. A rotation by $\frac{\pi}{4}$ on ϕ_j and ϕ_a, corresponds to a partial excitation. Adding such a determinant is used as our initial guess.
The choice of j and a that produce the best starting point is non-trivial. In preliminary calculations, we have done CC-calculations to see which excited state contributes the most to the wave function, as a guide in our choice. A better procedure would be to use the orbital energy differences (the denominator in the expression for the perturbation energy) and sort these in order of size. If when adding n determinants to the previously optimized reference state, the n lowest orbital energy differences would be used. Each would correspond to a partial excitation, or mixing of one occupied and one virtual orbital.

14.4 Optimization

An optimization procedure requires the calculation of the gradient of the energy with respect to the variational parameters. Using the analytical gradient is by far the fastest approach. However, the calculation is quite involved and we have not yet completed this part of the program. A routine that calculates the numerical gradient is also included in the program. In the final version, this will only be used to verify the analytical gradient, however, until the analytical gradient is available, the wave function can be optimized with the numerical gradient. This approach is equally accurate, but considerably slower. In the program, we employ the Broyden-Fletcher-Goldfarb-Shanno (BFGS) method with a numerical gradient calculated using the central differences method.

14.4.1 Central differences

The central differences method is used to calculate the numerical gradient of a function $f(x)$. The simplest case is a two point formula. This requires that $f(x+h)$ and $f(x-h)$ can be evaluated, where h is the chosen step size. Consider the Taylor expansion around the two points

$$f(x+h) = f(x) + f'(x)h + \frac{f^{(2)}(x)h^2}{2!} + \dots$$
$$f(x-h) = f(x) - f'(x)h + \frac{f^{(2)}(x)h^2}{2!} + \dots$$

Subtracting the second formula from the first and rearranging yields

$$f'(x) = \frac{f(x+h) - f(x-h)}{2h} \tag{14.4.1}$$

The two point formula has a truncation error $O(h^2)$. The accuracy of the formula can be increased by including more points, symmetrically spaced around x.

14.4.2 BFGS

The BFGS method is a method used for nonlinear optimization without constraints. The algorithm searches for stationary points on a multidimensional surface. The algorithm works as follows

1. An initial guess, $\mathbf{x}_0$ and an approximation to the Hessian matrix B_0 is given

2. A direction vector, $\mathbf{p}_x$ is obtained from the equation

$$B_k \mathbf{p}_k = -\nabla f(\mathbf{x}_k)$$

3. Along the determined direction, a line search determines the step length a_k and the solution vector is updated

$$\mathbf{x_{k+1}} = \mathbf{x_k} + a_k \mathbf{p}_k$$

4. $\mathbf{s}_k$ and $\mathbf{y}_k$ are given the values

$$\begin{aligned} \mathbf{s}_k &= a_k \mathbf{p}_k \\ \mathbf{y}_k &= \nabla f(x_{k+1}) - \nabla f(x_k) \end{aligned}$$

5. Finally, the approximation of the Hessian for the next step is calculated as

$$B_{k+1} = B_k + \frac{\mathbf{y}_k \mathbf{y}_k^T}{\mathbf{y}_k^T \mathbf{s}_k} - \frac{B_k \mathbf{s}_k (B_k \mathbf{s}_k)^T}{\mathbf{s}_k^T B_k \mathbf{s}_k} \tag{14.4.2}$$

6. Steps 2-5 are repeated until a convergence criteria is satisfied.

Our optimization problem can depend on a high number of variables, depending on the number of determinants used. The memory available is also limited and we have therefore chosen to use the limited memory BFGS, L-BFGS. This is a variation of the method described above. Instead of storing the whole approximate Hessian, the approximate Hessian is stored in the form of a few vectors, which represent the matrix implicitly. For systems with many variables, this can save considerable memory.

Chapter 15

Computational Methods

Dalton

Dalton is an open-source program package for quantum chemistry calculations. The program is written in Fortran and used by scientists all over the world. It contains modules for calculating energies and optimizing geometries using HF, MBPT, CC and DFT. The NOSD method uses the HF wave function as a starting point and it therefore convenient for us to implement our code in Dalton. We have added our code as a module that can be called from normal dalton-input files.

15.1 Implementation of NOSD in Dalton

This section outlines the NOSD-calculation in Dalton based on the equations from Chapter 14.

15.2 Driver

Since the NOSD-method uses the HF determinant as a starting point, a HF-calculation always preceds the NOSD-calculation in Dalton. After the HF-calculation is complete, a program called the NOSD-driver is called. The driver controls the calculation and runs the following tasks:

1. An initial guess is created
2. The energy of initial guess is calculated
3. The wave function is optimized with respect to the variational parameters

15.2.1 Initiating the calculation

In Section 14.3 the method of initiating the optimization is described. A rotated version of the HF reference determinant is added to the previously optimized determinant. At the present stage we hard-code the rotational parameters $\{\lambda_{bj}\}$ to be $\frac{\pi}{4}$. The number of determinants to be added to the reference state is controlled by input from the user.

15.2.2 Energy calculation

After the λ-matrix is initiated, the energy of the initial guess is calculated by a separate subroutine. The energy is calculated as follows:

1. The $D(\phi_n)$-matrices are calculated for all the determinants $\{\phi_n\}$ that are added to the reference wave function.
2. One- and two-electron integrals, h_{pq} and $(pq|rs)$ are stored during the HF-calculation and can be read from file.

3. The function $M(pq|rs)$ is calculated from the two electron integrals according to Equation (14.1.33).

4. The g-matrix is calculated from the D-matrices and the SVD of the overlap (Equation (14.1.17)).

5. The Hamiltonian matrix is calculated by contracting the M-integrals with the g-matrix and adding the one-electron contribution as in Equation (14.1.34).

6. From the Hamiltonian matrix the energy is calculated. This can be done in two ways:

   a) From the expectation value of the Hamiltonian as in Equation (14.1.36)
   b) From the eigenvalues of the diagonalized Hamiltonian.

   The energy is calculated using the expectation value of the Hamiltonian, except in the first calculation of the energy of the initial guess.

7. Lastly the nuclear contribution from the HF calculation is added and the total energy is given.

15.2.3 Optimization

After the energy of the initial guess is calculated, the optimization begins. This is done using an L-BFGS-routine. The energy and gradient are inputs in the optimization. The energy is calculated as described above and the gradient is calculated using the central differences method (Section 14.4.1). The L-BFGS-routine is independent of the gradient procedure. At a later stage, a routine for calculating the analytical gradient will be implemented, which will increase the speed of the optimization.

Chapter 16

Results and discussion of NOSD results

The NOSD code has been tested for two systems, Be_2 and water. Computations are quite slow since the optimization has to be done using the numerical gradient. This limits the number of determinants we can add to the HF wave function. The results described in this Chapter are preliminary as the program is not completed yet.
For both test systems we have calculated the energy with two and three determinants. This means that one and two determinants are added to the HF state, respectively. Initial results indicate that when using more than two determinants, situations where the norm of the wave function approaches zero can occur. To avoid this, we have also done calculations where the HF-reference is kept fixed during the optimization. This is only a temporary solution to the problem. We are currently investigating a permanent solution, where all added determinants are orthogonal to the HF state in the initial guess.

16.1 Water

Potential energy curves for water during symmetric stretching of the OH bond is presented in [64] using HF, MP2, CCSD(T) and FCI. In Figure 16.1 these results are compared to NOSD calculations using two and three determinants (for two determinants, results from calculations with a fixed HF reference and results where it is unrestricted are shown). The graph shows the total energy. The experimental value of the O-H bond length is 0.976 Å.

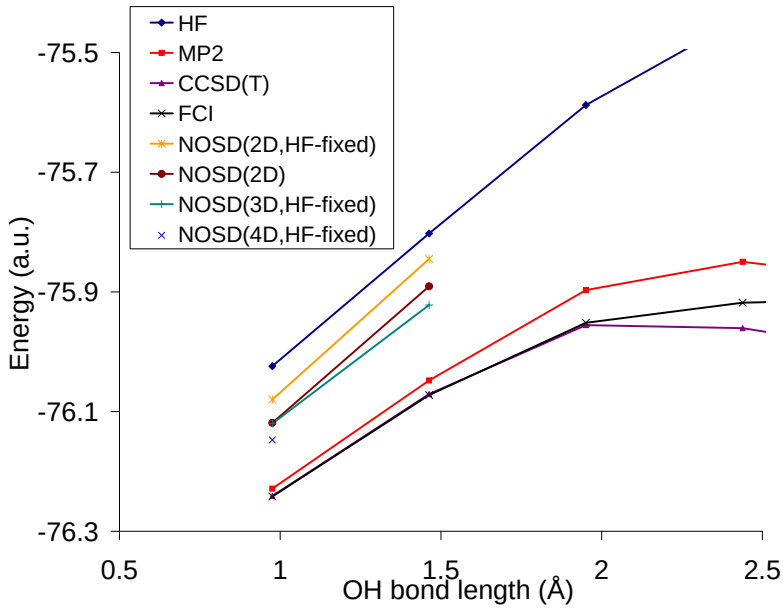

Figure 16.1: Energy curve of water under symmetric stretching of the O-H bond calculated with various methods

A measure of the accuracy of NOSD is the percentage of electron correlation recovered. The correlation energy in the NOSD calculations

of water in the equilibrium geometry are presented in Table 16.1

Table 16.1: Correlation energy (a.u.) for H_2O calculated by NOSD with two and three determinants. NOSD calculations are carried out the cc-pVDZ basis set.

Method	Correlation energy	%
FCI [64]	-0.218	100
NOSD(2D,HF-fixed)	-0.056	25.7
NOSD(2D)	-0.095	43.6
NOSD(3D,HF-fixed)	-0.096	44.1
NOSD(4D,HF-fixed)	-0.124	56.9

When the NOSD was tested in 1993, 67% of the correlation energy was recovered by using 5 determinants. This was however done using a smaller basis set than we have, so the results are not directly comparable. However, the trend in correlation energy with increasing number of determinants is very encouraging.

16.2 Be_2

Using the beryllium dimer, we have tested the NOSD-method with two and three determinants. In Table 16.2 the results from NOSD calculations are listed along with experimental values from [69] and FCI-results from [68]. We have also included calculations from this study with HF, MP2, CCSD and CCSD(T)-methods and the cc-pVDZ basis set. These calculations have been done using CFOUR.
The whole potential energy curves for the Be_2 dimer, calculated with various methods in this study are shown in Figure 16.2. HF, MP2, CCSD and CCSD(T) calculations are done using CFOUR [37]. The experimental value reported by Merritt [69] is also included. This value is almost identical to the FCI/CBS-value from [68].

Table 16.2: The binding energy at the experimental bond length (2.44 Å), the calculated bond length and the binding energy at the calculated bond length. Energies in cm^{-1} and bond lengths in Å. Calculations from this study are done with the cc-pVDZ basis set.

Method	Binding energy at 2.44 Å	Calculated bond length	Binding energy at calculated bond length
Experimental [69]	-930	-	-
FCI/CBS [68]	-938 ± 15	2.44	-
HF	+2750	6.41	-1.48
MP2	+327	4.29	-103.42
CCSD	+818	5.00	-34.22
CCSD(T)	+128	4.54	-60.28
NOSD(2D)	+1881	4.43	-146.00
NOSD(3D)	-571	-	-

The results shown in Table 16.2 and Figure 16.2 clearly show how poorly HF, MP2, CCSD and CCSD(T) describe the beryllium dimer. Among these standard methods, the best correspondence with experiments and FCI is actually shown by MP2. Although these results are better than the other, they are very inaccurate; the bond length is 76% longer than the experimental and the binding energy is only 11% of the experimental result. The NOSD(2D)-results are also inaccurate, however, the binding energy (-146 cm^{-1}) is considerably more accurate than the standard methods, and the bond length is almost as accurate as the MP2 calculations. This is obtained by only adding one, non-orthogonal determinant to the HF state. The improvement in binding energy at 2.44 Å of NOSD(2D) over HF corresponds to a recovery of 23.6% of the correlation energy. This is approximately half of what was obtained for water using two determinants. Using three

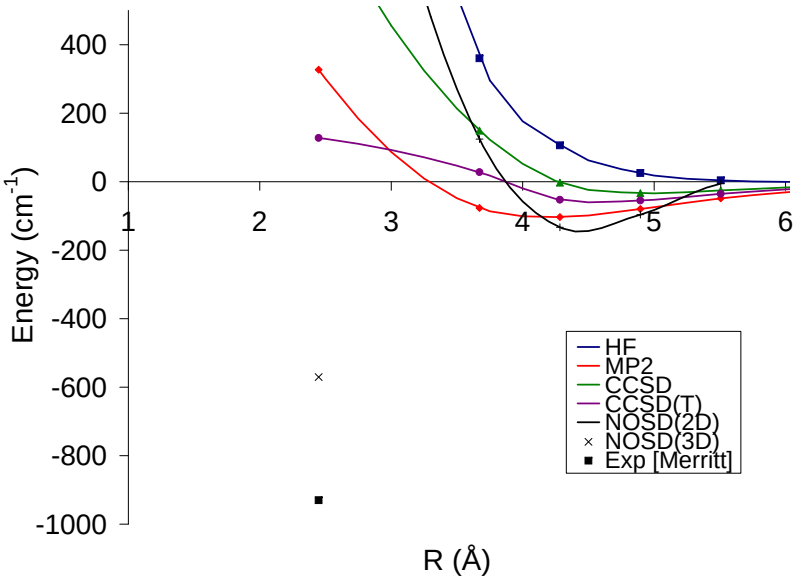

Figure 16.2: Potential energy curve of the beryllium dimer calculated with various methods

determinants, we have only calculated two points, one at the experimental bond length and at the dissociation energy. This results in a binding energy of -571 cm^{-1} at 2.44 Å. This is a drastic improvement compare to the other results shown in Figure 16.2. The binding energy represents recovery of 90% of the correlation energy. For this system, the correlation energy is very large, and despite recovering 90%, there is still a difference of 360 cm^{-1}. It should also be noted that we are comparing the NOSD-energies to FCI calculations extrapolated to the complete basis set limit. This means that part of the discrepancy between our result and the FCI-energy is also due to basis set trun-

cation error. The binding energy at the experimental bond length as calculated by NOSD(3D) represents a vast improvement compared to the MP2, CCSD and CCSD(T) results. Unfortunately, we have not had time to calculate the entire potential energy curve using three determinants.

Chapter 17

Conclusion

The description of the NOSD-method in the original Letter by Koch and Dalgaard is very condensed. We hope that the presentation of the fundamental theory and the details of the method have been more clearly described in Chapters 14 and 15.

Although the NOSD-code is not yet complete, the preliminary results presented in Chapter 16 illustrate its potential. For the water molecule, the energy calculated with NOSD is much more accurate than the HF-energy, even by adding only one determinant. Without adding more determinants, the accuracy of NOSD cannot compare with MP2 or CCSD(T), however the results from [61] indicate that a very high accuracy can be expected when the code is code is complete and a higher number of determinants can be used. For the Be_2 molecule, the results from NOSD(2D)-calculations are of a comparable accuracy to that of MP2 and CCSD(T). Compared to the experimental and FCI results, this is still not very accurate. Using three determinants shows a radical improvement in the binding energy at the experimental bond length compared to the other methods. If the results show the same rate improvement when more determinants are

added, there is reason to hope for results close to FCI-accuracy when the program is completed.

Chapter 18

Future work

As mentioned in the Discussion, the implementation of NOSD in Dalton has not been completed. The goal was to finish the implementation within the end of this project, however, the programming and testing proved to require more time than expected. The most important remaining parts of the program are to calculate the analytical gradient and to implement a stabile and robust method of initiating the calculations. With only the numerical gradient, calculations are very slow which has limited the test calculations. When the analytical gradient is available, test calculations can be conducted faster and more extensive results can be presented. We also wish to add a section for analysis of the calculations in the program. This will include the diagonalization of the one-electron density which will give the natural occupation, and a presentation of the two-electron density. Work to finish the program is currently ongoing and will be a part of my PhD-project.

Appendices

Appendix A

DFT potential energy curves from Part A

In this appendix, the potential energy curves of the DFT functionals that were not shown in Chapter 5 are displayed. The DFT energies are calculated using ADF and the TZ2P basis set. For each geometry, the CCSD(T)/cc-pVTZ energy curve is included for comparison.

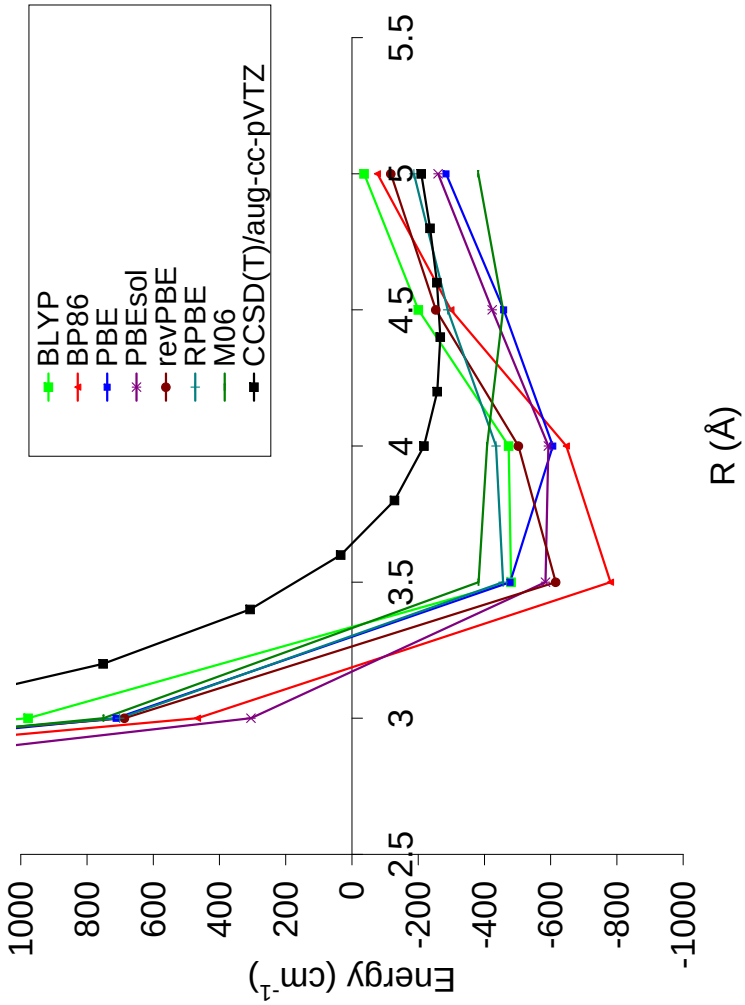

Figure A.1: The DFT potential energy curves of benzene and a sodium dimer in the parallel geometry (Figure 4.1). for DFT functionals not discussed in Chapter 5

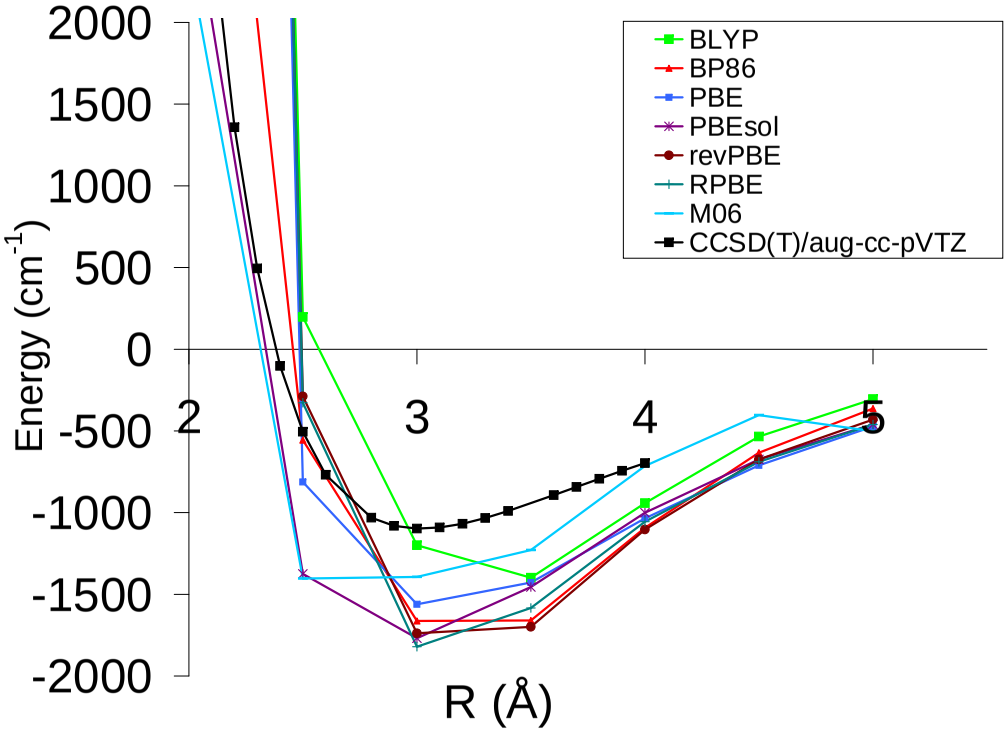

Figure A.2: The DFT potential energy curves of benzene and a sodium dimer in the parallel geometry (Figure 4.1). for DFT functionals not discussed in Chapter 5

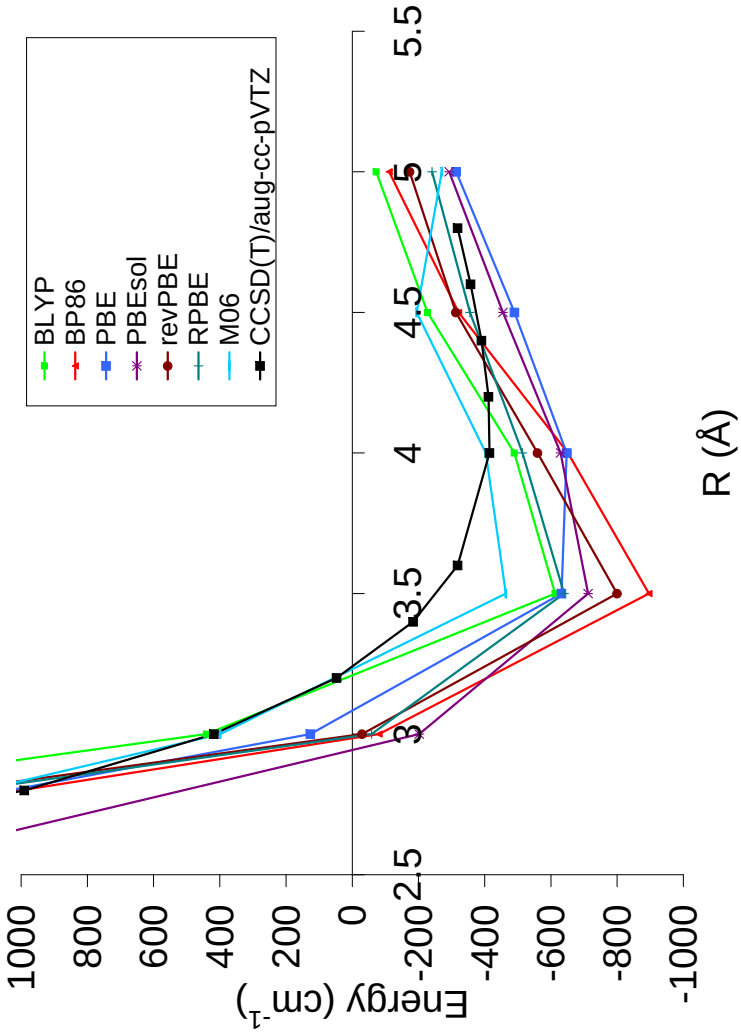

Figure A.3: The DFT potential energy curves of benzene and a sodium dimer in the parallel geometry (Figure 4.1) for DFT functionals not discussed in Chapter 5.

Appendix B

Structural parameters from Part B

In this appendix, the structural parameters of the molecules investigated in Part B of this thesis are listed. 1,2-dichloro and 1,2-difluoro ethane were discussed in Section 10 and are not listed here.

Table B.1: Structural parameters of halo(halomethyl)silanes investigated in Part B of this thesis. All bond lengths are in Å and bond angles in degrees. Geometry optimizations are carried out with cc-pVDZ basis sets. The torsional angle (Cl-Si-C-Cl) was kept fixed at 180^o in optimizations of anti-conformers.

Fluoro(fluoromethyl)silane(FH_2C-SiH_2F)						
	Anti			Gauche		
	HF	MP2	CCSD(T)	HF	MP2	CCSD(T)
Si-C	1.895	1.894	1.900	1.892	1.897	1.893
C-F	1.385	1.408	1.410	1.401	1.404	1.380
Si-F	1.637	1.654	1.654	1.651	1.652	1.634
F-C-Si	107.0	105.1	105.2	109.4	109.3	109.8
F-Si-C	106.6	108.7	108.5	109.5	109.4	108.9
F-Si-C-F	180.0	180.0	180.0	71.1	69.2	69.3
Chloro(chloromethyl)silane(ClH_2C-SiH_2Cl)						
	Anti			Gauche		
	HF	MP2	CCSD(T)	HF	MP2	CCSD(T)
Si-C	1.893	1.891	1.897	1.894	1.893	1.899
C-Cl	1.808	1.800	1.815	1.801	1.795	1.809
Si-Cl	2.093	2.085	2.091	2.083	2.076	2.083
Cl-C-Si	108.3	107.4	107.3	111.7	110.9	110.9
Cl-Si-C	107.1	108.1	108.2	109.5	109.4	109.6
Cl-Si-C-Cl	180.0	180.0	180.0	68.8	66.3	66.7

Table B.2: Structural parameters of 1,2-dihalodisilanes investigated in Part B of this thesis. All bond lengths are in Å and bond angles in degrees. Geometry optimizations are carried out with cc-pVDZ basis sets. The torsional angle (F-Si-Si-F) was kept fixed at 180^o in optimizations of anti-conformers.

1,2-difluorodisilane($FH_2Si-SiH_2F$)						
	Anti			Gauche		
	HF	MP2	CCSD(T)	HF	MP2	CCSD(T)
Si-Si	2.367	2.358	2.361	2.367	2.356	2.359
Si-F	1.643	1.661	1.661	1.640	1.658	1.659
F-Si-Si	106.7	107.2	107.2	108.5	109.4	109.4
F-Si-Si-F	180.0	180.0	180.0	73.2	70.9	71.4
1,2-dichlorodisilane($ClH_2Si-SiH_2Cl$)						
	Anti			Gauche		
	HF	MP2	CCSD(T)	HF	MP2	CCSD(T)
Si-Si	2.364	2.350	2.355	2.368	2.353	2.357
Si-Cl	2.101	2.093	2.101	2.095	2.088	2.096
Cl-Si-Si	107.3	107.5	107.7	108.7	107.9	108.3
Cl-Si-Si-Cl	180.0	180.0	180.0	67.5	64.0	64.3

Bibliography

[1] A. Szabo and N. Ostlund, *Modern Quantum Chemistry*, Dover Books, 1989.

[2] T. Helgaker, P. Jørgensen, and J. Olsen, *Molecular Electronic Structure Theory*, Chapter 1, First Edition, Wiley, 2000.

[3] A. Szabo and N. Ostlund, *Modern Quantum Chemistry*, Chapter 2, Dover Books, 1989.

[4] W. Heisenberg, *Z. Phys.* **43**, 172 (1927).

[5] J. Slater, *Phys.Rev.* **34**, 1293 (1929).

[6] E. U. Condon, *Phys. Rev.* **36**, 1121 (1930).

[7] H. Baker, *Proc Lond Math Soc* **34**, 347 (1902).

[8] F. Hausdorff, *Ber Verh Saech Akad Wiss Leipzig* **58**, 19 (1906).

[9] J. Campbell, *Proc Lond Math Soc* **28**, 381 (1897).

[10] H. Poincare, *Compt Rend Acad Sci Paris* **128**, 1065 (1899).

[11] T. Helgaker, P. Jørgensen, and J. Olsen, *Molecular Electronic Structure Theory*, Chapter 5, First Edition, Wiley, 2000.

[12] T. Helgaker, P. Jørgensen, and J. Olsen, *Molecular Electronic Structure Theory*, Chapter 13, First Edition, Wiley, 2000.

[13] T. Dunning, *J. Chem. Phys.* **90**, 1007 (1989).

[14] T. Helgaker, P. Jørgensen, and J. Olsen, *Molecular Electronic Structure Theory*, Chapter 8, First Edition, Wiley, 2000.

[15] A. Halkier, T. Helgeaker, P. Jørgensen, W. Klopper, H. Koch, J. Olsen, and A. K. Wilson, *Chemical Physics Letters* **286**, 243 (1998).

[16] S. F. Boys and F. Bernardi, *Mol. Phys.* **19**, 553 (1970).

[17] F. M. Tao, *J. Chem. Phys.* **98**, 3049 (1993).

[18] P. Hohenberg and W. Kohn, *Phys. Rev.* **136**, B864 (1964).

[19] W. Kohn and L. J. Sham, *Phys. Rev.* **140**, A1133 (1965).

[20] C. Lee, W. Yang, and R. G. Parr, *Phys. Rev.* **37**, 785 (1988).

[21] A. D. Becke, *Phys. Rev.* **38**, 3098 (1988).

[22] J. Tao and J. P. Perdew, *Phys. Rev.* **91**, 146401 (2003).

[23] A. D. Becke, *J. Chem. Phys.* **98**, 1371 (1993).

[24] S. Grimme, J. Antony, S. Ehrlich, and H. Krieg, *J. Chem. Phys.* **132**, 154104 (2010).

[25] K. Grjotheim and H. Kvande, *Introducction to Aluminium Electrolysis*, Aluminium Verlag, 1993.

[26] H. A. Øye and B. J. Welch, *JOM* **50**, 18 (1998).

[27] F. A. Kozlov, V. V. Alekseev, E. A. Orlova, N. V. Gavrilova, and Y. P. Kovalev, *Atomic Energy* **101**, 887 (2009).

[28] Y. Mikhalev and H. A. Øye, *Carbon* **34**, 37 (1996).

[29] Z. Wang, J. Rutlin, and T. Grande, *Light Metals* , 841 (2010).

[30] H. Eyring, *J. Chem. Phys.* **3**, 107 (1935).

[31] A. F. Voter, *Introduction to the Kinetic Monte Carlo Method, in Radiation Effects in Solids*, Springer, NATO Publishing Unit, 2005.

[32] H. Mehrer, *Diffusion in Solids*, Chapter 4, First Edition, Springer Series in Solid-State Sciences, 2007.

[33] G. Boisvert and L. J. Lewis, *Phys. Rev.* **54**, 2880 (1996).

[34] M. R. Sørensen and A. F. Voter, *J. Chem. Phys.* **112**, 9599 (2000).

[35] T. Naas, *C. E. Eckert, Editior, Light metals*, The Minerals, Metals and Materials Society, 1999.

[36] G. J. Houston, B. J. Welch, and D. J. Young, *B. Welch, Editior, Light metals*, The Metallurgical Society of AIME, 1998.

[37] J. Stanton, J. Gauss, M. E. Harding, and P. G. Szalay, CFOUR, Coupled-Cluster techniques for Computational Chemistry, Software, 2010.

[38] G. te Velde, F. M. Bickelhaupt, E. J. Baerends, C. F. Guerra, S. J. A. va Gisbergen, J. G. Snijders, and T. Ziegler, *J. Comp. Chem.* **22**, 931 (2001).

[39] S. Andersson, Unpublished DFT calculations of benzene and sodium dimer, 2010.

[40] J. G. Hop, *Sodium Expansion and creep of Cathode Carbon*, PhD thesis, NTNU, 2003.

[41] T. Grande, Discussions.

[42] S. J. Squea, R. Jones, and P. R. Briddon, *Phys. Status Solidi A* **204**, 3078 (2007).

[43] T. A. baker and M. Head-Gordon, *J. Phys. Chem. A* **114**, 10326 (2010).

[44] R. Stølevik, *J. Mol. Struct.* **291**, 301 (1993).

[45] R. Stølevik and K. Hagen, *J. Mol. Struct.* **352/353**, 25 (1995).

[46] F. Akkerman, J. Buschmann, D. Lentz, P. Luger, and E. Rödel, *J. Chem. Cryst.* **33**, 969 (2003).

[47] R. K. Sreeruttun and P. Ramasami, *Phys. Chem. Liq.* **44**, 315 (2006).

[48] R. Stølevik, Unpublished molecular mechanics calculations of conformational energies of 1,2-dihalodisilanes and halo(halomethyl)silanes, 1995.

[49] L. S. Bartell, *J. Chem. Phys.* **38**, 1827 (1963).

[50] P. Ramasami, volume 1, pp. 1139–1146, 2010.

[51] B. Bhonoah, A. Ghoorun, H. H. Abdallah, and P. Ramasami, *J. Sol. Chem.* **40**, 430 (2011).

[52] HyperChem(TM) 8, Software. Hypercube, Inc., 1115 NW 4th Street, Gainesville, Florida 32601, USA.

[53] M. E. Harding, T. Metzroth, J. Gauss, and A. A. Auer, *J. Chem. Theor. Comp.* **4**, 64 (2008).

[54] J. R. Durig, J. Liu, and T. S. Little, *J. Phys. Chem.* .

[55] K. Kveseth, *Acta Chem. Scand.* **29**, 307 (1975).

[56] H. Takeo and C. Matsumura, *J. Chem. Phys.* **84**, 4205 (1986).

[57] D. Freisen and K. Hedberg, *J. Am. Chem. Soc.* **102**, 3987 (1980).

[58] P. Pyykko and J. P. Desclaux, *Acc. Chem. Res.* **12**, 276 (1979).

[59] A. Rutkowski, *J. Phys. B: At. Mol. Phys.* **19**, 149 (1986).

[60] S. A. Perera and R. J. Bartlett, *Chemical Physics Letters* **216**, 606 (1993).

[61] H. Koch and E. Dalgaard, *Chemical Physics Letters* **212**, 193 (1993).

[62] H. Koch, Discussions.

[63] DALTON, a molecular electronic structure program, Release 2.0 (2005), see http://www.kjemi.uio.no/software/dalton/dalton.html.

[64] J. Olsen, P. Jørgensen, H. Koch, A. Balkova, and R. J. Bartlett, *J. Chem. Phys.* **104**, 8007 (1996).

[65] S. Fraga and B. J. Ransil, *J. Chem. Phys.* **35**, 669 (1961).

[66] S. Fraga and B. J. Ransil, *J. Chem. Phys.* **36**, 1127 (1962).

[67] C. F. Bender and E. R. Davidson, *J. Chem. Phys.* **47**, 4972 (1967).

[68] K. Patkowski, R. Podeszwa, and K. Szalewicz, *J. Phys. Chem. A* **111**, 12822 (2007).

[69] J. M. Merritt, V. E. Bondybey, and M. C. Heaven, *SCIENCE* **324**, 1548 (2009).